Journal of Inflammation Research

Dovepress
Taylor & Francis Group

Open Access Full Text Article

ORIGINAL RESEARCH

Exploring Potential Causal Links: How Parkinson's Disease Brain Damage Impacts Liver Health–A Mendelian Randomization and Transcriptomic Study

Tingting Liu[1,2,*], Qi Chen[3,*], Haojie Wu[1], Jingwen Li[1], Meiyan Xian[1], Keke Lu[1,2], Chaoyang Zhu[1,2], Jianshe Wei[1,2]

[1]School of Life Sciences, Henan University, Kaifeng, People's Republic of China; [2]Translational Neuromedicine and Neurourology Center, Huaihe Hospital of Henan University, Kaifeng, People's Republic of China; [3]School of Traditional Chinese Pharmacy, China Pharmaceutical University, Nanjing, People's Republic of China

*These authors contributed equally to this work

Correspondence: Jianshe Wei, Email jswei@henu.edu.cn

Journal of Inflammation Research downloaded from https://www.dovepress.com/
For personal use only.

Background: Parkinson's disease (PD) is a common neurodegenerative disorder characterized by slow movements, muscle rigidity, tremors, and changes in gait and posture. Clinical studies have demonstrated a close association between PD and liver disease, but most research has focused on the impact of liver disorders on brain damage in PD, and further exploration is needed to understand the pathways and mechanisms underlying liver damage in patients with PD.

Methods: This study employs Mendelian Randomization (MR) and transcriptomic analysis to investigate the causal impact of PD-related brain damage on liver health, identifying serum metabolites (eg, cysteine) and shared immune-inflammatory pathways as mediators.

Results: The study indicates that PD-related brain damage does indeed have an impact on liver metabolic function. PD-related brain damage may disrupt the concentration of cysteine, which, when elevated, can cause liver cell damage and oxidative stress. Additionally, PD-related brain damage may affect specific genes (such as NCF1, NCF, and SELPLG) involved in immune and inflammatory responses that lead to liver damage. Interestingly, the anti-PD drug, tolcapone, has notable therapeutic effects but also negatively affects specific genes, contributing to liver damage in patients with PD.

Conclusion: This study reveals the mechanisms by which PD affects liver metabolism and proposes cysteine as a biomarker and therapeutic target for liver damage in PD. Furthermore, the impact of PD treatment drugs on liver function was also evaluated. These findings provide important insights for the development of future PD treatment strategies, and further clinical research is needed to validate and optimize clinical interventions to maximize treatment efficacy and minimize side effects in patients with PD.

Keywords: Parkinson's disease, chronic hepatitis, Mendelian randomization analysis, serum metabolites, cysteine

Introduction

Parkinson's disease (PD) is clinically defined by movement-related manifestations such as slowed movements (bradykinesia), muscle stiffness, resting tremors, and impaired balance coordination, which together constitute parkinsonism.[1] Ranking as the second most common neurodegenerative condition after Alzheimer's disease, PD demonstrates the fastest-growing epidemiological burden among neurological disorders, currently affecting more than six million individuals globally.[2] Although advancing age remains the primary risk determinant, modifiable environmental exposures and behavioral patterns significantly contribute to the development of age-associated neurodegenerative conditions.[3] The neuropathological hallmarks of PD include progressive loss of dopamine-producing neurons in the substantia nigra pars compacta (SNpc) coupled with abnormal aggregation of α-synuclein (α-syn) proteins forming characteristic Lewy bodies

Received: 16 December 2024
Accepted: 16 June 2025
Published: 21 June 2025

© 2025 Liu et al. This work is published and licensed by Dove Medical Press Limited. The full terms of this license are available at https://www.dovepress.com/terms.php and incorporate the Creative Commons Attribution – Non Commercial (unported, v4.0) License (http://creativecommons.org/licenses/by-nc/4.0/). By accessing the work you hereby accept the Terms. Non-commercial uses of the work are permitted without any further permission from Dove Medical Press Limited, provided the work is properly attributed. For permission for commercial use of this work, please see paragraphs 4.2 and 5 of our Terms (https://www.dovepress.com/terms.php).

(LBs) inclusions.[4] Disease progression involves multiple pathogenic mechanisms including oxidative stress from excessive free radicals, disrupted cellular energy metabolism, and compromised mitochondrial functionality, all contributing to the selective degeneration of dopaminergic neurons.[5]

Recent clinical evidence indicates a significant connection between the central nervous system (CNS) and liver diseases, particularly in patients with PD.[6,7] Understanding the interrelationship between the CNS and liver diseases is essential for assessing the overall condition and disease progression in patients with PD. Clinical data suggest that as neurodegenerative disorders progress, the liver, a critical organ for maintaining metabolic homeostasis, is the first to show functional impairment, followed by the kidneys and heart.[8] The liver plays a vital role in various physiological activities, including cholesterol homeostasis, immune support, protein synthesis, and whole-body metabolism.[9] This organ is composed of highly diverse groups of cells that work together to carry out the organ's functions in both healthy and diseased individuals.[10] Studies have demonstrated that several metabolic disorders, including PD, are associated with dysregulation of liver-related physiological processes.[11] Liver P450 subsystem damage has been reported in patients with delayed-onset PD.[12,13] The liver is pivotal in maintaining the homeostasis of whole - body glutathione (GSH), and among all organs, it holds the highest GSH concentration.[14] GSH is of great significance in the cellular antioxidant defense system and the detoxification process.[15] The availability of cysteine is a key factor influencing GSH synthesis. Conversely, in specific cell types, an abnormally high level of cysteine can give rise to oxidative stress and cytotoxicity.[16] Additionally, Squitti et al[17] reported that patients with PD residing near iron alloy factories had elevated levels of aspartate aminotransferase (AST) and alanine aminotransferase (ALT), along with subclinical liver dysfunction.

Emerging studies indicate that hepatic dysfunction in PD patients may intensify cerebral damage, mirroring the pathophysiological mechanisms observed in acquired hepatocerebral degeneration (AHD). This neurological disorder, typically associated with end-stage liver cirrhosis (LC) or portosystemic shunting, manifests through progressive motor abnormalities and cognitive deficits similar to those seen in advanced PD cases. Movement disorders are the most common neurological manifestations of AHD, with approximately 20% of patients with AHD exhibiting parkinsonism. The exact pathophysiology of AHD remains unclear. None of the proposed hypotheses encompass all the plausible mechanisms believed to contribute to its development. Emerging evidence points to compromised hepatic detoxification pathways as a critical driver in acquired hepatocerebral degeneration (AHD), where impaired toxin elimination—particularly manganese and ammonia—creates a neurotoxic milieu. While hyperammonemia was historically emphasized in AHD pathogenesis, contemporary research prioritizes manganese dysregulation as a central mechanistic framework. The neurotoxic effects of ammonia appear mediated through astrocytic dysfunction, specifically disrupting the glutamate-glutamine cycle. This process critically depends on glutamine synthetase activity, an astrocyte-specific enzyme essential for converting glutamate to glutamine, thereby maintaining cerebral excitatory neurotransmission homeostasis.[18] The increase in ammonia concentration in chronic liver disease inhibits the clearance of glutamine by astrocytes through glutamine synthetase, leading to the accumulation of glutamine and mild cerebral edema.[19] Overall, liver damage exacerbates brain injury in PD. However, the impact of brain injury on liver function in patients with PD, considering the intricate interplay between the liver and the brain, remains insufficiently studied.

This study presents groundbreaking evidence for a bidirectional causal relationship between PD-related brain injury and liver dysfunction through an innovative combination of Mendelian randomization (MR) and transcriptomic analysis. Leveraging genome-wide association study (GWAS) data, we employed bidirectional MR to systematically evaluate the PD-liver interaction, revealing serum cysteine as a crucial metabolic mediator that exhibits concentration-dependent effects - neuroprotective at low levels but hepatotoxic at elevated concentrations. Importantly, we identified specific immune-inflammatory hub genes (neutrophil cytosolic factor 1 (NCF1), spleen-associated tyrosine kinase (SYK)) through which the anti-PD drug tolcapone exerts its hepatotoxic effects, providing the first molecular explanation for its known liver injury risks.

The clinical implications of these findings are particularly significant given that PD patients typically require long-term pharmacotherapy with drugs like levodopa. Our multi-omics approach, integrating MR with transcriptomic profiling of PD and liver injury models, demonstrates that PD-associated brain injury can disrupt hepatic metabolic function through both circulating metabolites (cysteine) and shared molecular pathways. This systemic perspective advances our understanding of PD beyond its classical neurological manifestations, revealing it as a disorder of inter-organ communication. Methodologically, we employed a rigorous analytical pipeline: (1) bidirectional MR to establish causal

directions in the PD-liver axis; (2) serum metabolite analysis to identify cysteine as a key mediator; (3) transcriptomic comparison to uncover shared gene networks in PD and hepatitis B virus (HBV); and (4) experimental validation of hub genes in peripheral blood mononuclear cells (PBMCs) and liver cells. This comprehensive strategy not only confirms the brain-liver connection in PD but also provides clinically actionable biomarkers for monitoring hepatic health in PD patients undergoing long-term treatment, potentially enabling personalized medication regimens to minimize side effects while maintaining therapeutic efficacy. The flowchart of this study is presented in Figure 1.

Materials and Methods

MR Analysis

Establishment of the Program

The study design followed the basic principles of MR.[20,21] PD was initially treated as the exposure variable, while relevant liver injury diseases were considered outcome variables. Concurrently, serum metabolites were examined as outcome variables to identify the metabolites that PD may affect. Subsequently, these serum metabolites were further screened as exposure variables to determine their impact on the liver. The overall findings revealed the specific metabolic pathways through which PD affects the liver. During the analysis, stringent inclusion and exclusion criteria were applied, selecting single nucleotide polymorphisms (SNPs) significantly associated with the exposure target as instrumental variables (IVs) for two-sample MR. A series of sensitivity analyses were conducted on the statistically significant results. Notably, publicly available summary statistics from GWAS were used in this analysis, and the original GWAS was approved by the relevant institutional review boards.

Serum Metabolite Data

The serum metabolite GWAS involved comprehensive genetic association scans of 486 metabolites in 7,824 adult individuals from two European populations, resulting in complete GWAS statistical data for human blood metabolites. Utilizing structural and biochemical profiling, the metabolites were stratified into nine distinct biosignature clusters—eight encompassing principal biochemical superfamilies and one comprising unclassified entities. The defined categories spanned essential biomolecular domains: nitrogenous bases (nucleotides), nitrogen metabolism derivatives (amino acids/peptides), saccharide derivatives (carbohydrates), redox mediators (cofactors/vitamins), bioenergetic intermediates, lipid species, along with xenobiotic compounds.[22]

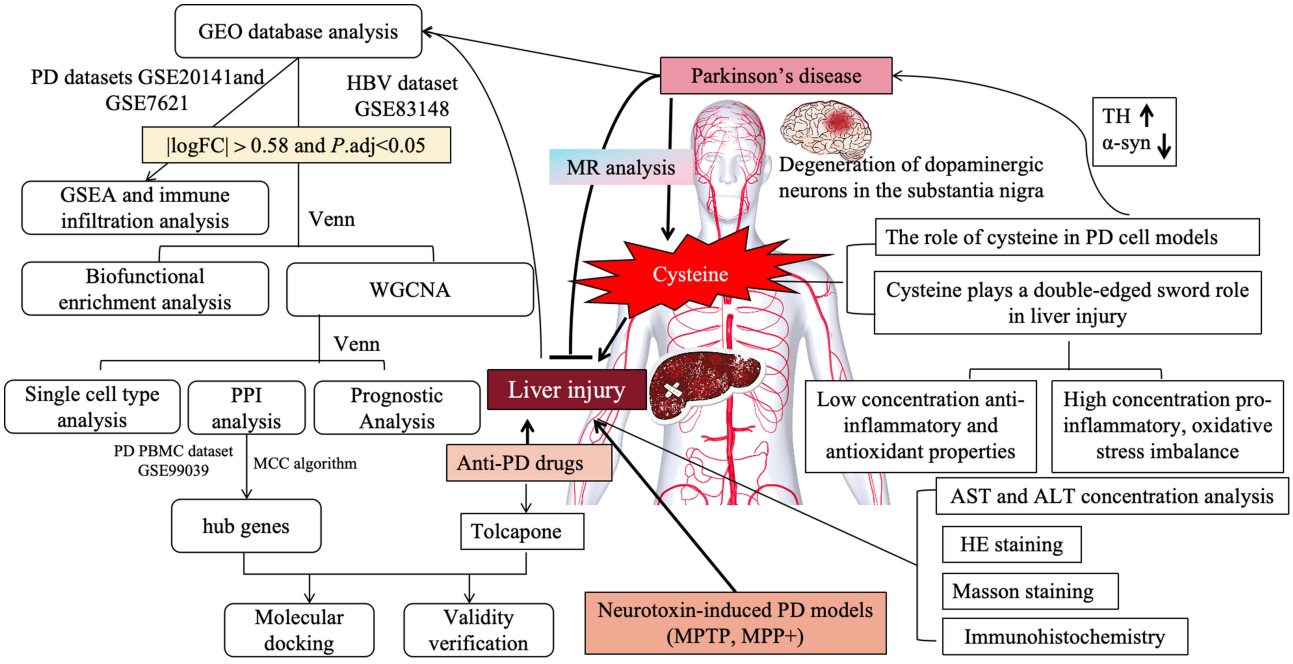

Figure 1 The flow chart of this study.
Abbreviations: GSEA, gene set enrichment analysis; WGCNA, Weighted correlation network analysis; PPI, protein-protein interaction networks.

https://doi.org/10.2147/JIR.S511645

PD and Hepatitis Sample Data

The GWAS data for diseases were obtained from the Open GWAS database (https://gwas.mrcieu.ac.uk/), which comprises at least 12.6 billion genetic associations from over 14,582 complete GWAS datasets, representing a diverse range of human phenotypes and disease outcomes across different populations. In this experiment, two types of diseases were included as the analysis targets: PD and liver injury-related diseases. Liver injury-related diseases include viral hepatitis (such as hepatitis B and hepatitis C), autoimmune hepatitis, nonalcoholic fatty liver disease, liver fibrosis and cirrhosis. In addition, it also includes GWAS data about liver function abnormalities. Specifically excluded were liver cancer and alcoholic fatty liver disease types, as their primary causes were not related to brain injury-related diseases. Detailed information on specific diseases is presented in Supplementary Table S1.

Selection of IVs

To obtain effective and significant SNPs as IVs, different treatments were applied when different targets were considered as exposures. When serum metabolites and PD were considered as exposures separately, the threshold for screening SNPs significantly associated with exposure was set at $P < 1\times10^{-5}$ and $P < 5\times10^{-8}$, respectively. Additionally, SNPs in linkage disequilibrium were excluded using the European population reference group from the 1000 Genomes Project, with parameters set as $r^2 < 0.01$ (500 kb) and $r^2 < 0.001$ (1000 kb). Furthermore, the selected SNPs were harmonized using summary data from GWAS outcomes, and any palindromic SNPs or SNPs not available in the GWAS results were discarded. The filtered SNPs were then utilized as final IVs MR analysis. To validate the instrumental strength assumption for the analysis, the proportion of exposure variance explained by genetic variation (R^2) was estimated using the following formula $R^2 \approx \sum_{i}^{K} \frac{\beta_i^2}{\beta_i^2+N(se(\beta_i))^2}$ where β_i represents the effect size of genetic instrument variable i, N is the effective sample size, se(β_i) is the standard error of the effect size for genetic variation i, and K is the number of independent genetic variations.[23] Additionally, the F-statistic was computed as $F = \frac{(N-K-1)R^2}{K(1-R^2)}$ and compared to an empirical threshold of 10 to assess the strength of these genetic instruments.[24]

Two-Sample MR

In bidirectional Mendelian randomization (MR) investigations, analytical approaches were stratified by genetic instrument complexity. For mono-SNP exposures, causal estimates were derived from the Wald ratio estimator, computed as the quotient of outcome-associated to exposure-associated SNP effects. Poly-SNP instruments employed inverse variance-weighted (IVW) meta-analyses under fixed/random effects paradigms, supplemented by pleiotropy-robust methodologies including weighted median estimator, MR-Egger regression, and simplified/weighted modeling frameworks to validate result stability.[25] Instrumental variable (IV) heterogeneity was quantified through Cochrane's Q statistics, with random-effects IVW implementation when exceeding statistical significance threshold (α=0.05). The weighted median approach maintained estimation consistency when valid IVs contributed >50% analytical weight,[26] whereas MR-Egger accommodated directional pleiotropy even under majority invalid IV scenarios.[27] Outlier detection via MR-PRESSO enabled IVW estimate correction through iterative exclusion of heterogeneous variants, complemented by leave-one-out sensitivity analyses to identify SNP-driven result distortions.

All computations were implemented through R v4.0.3, utilizing TwoSampleMR for core MR methodologies (IVW, weighted median, MR-Egger) and MRPRESSO for outlier detection protocols.

Analysis of Differentially Expressed Genes (DEGs) in PD and HBV Based on GEO Database

DEGs Acquisition

Parkinson's disease transcriptomic profiles were sourced from GEO repositories (GSE20141/GSE7621; 26 PD cases vs 17 controls), while hepatitis B virus (HBV) data derived from GSE83148 (122 hBV-infected individuals vs 6 controls). All microarray datasets were profiled on the Affymetrix HG-U133 Plus 2.0 array (GPL570). Differentially expressed genes were identified using stringent thresholds (|logFC| > 0.58 and *P*.adj < 0.05). Validation cohorts encompassed PD series (GSE20163/GSE20164/GSE99039) and HBV datasets (GSE38941/GSE58208), with comprehensive cohort characteristics detailed in Table 1.

Table 1 The Detailed Information of the Dataset

Dataset	Platform	Information
GSE20141	GPL570[HG-U133_Plus_2] Affymetrix Human	10 PD brain samples and 8 control brain samples of SN pars compacta neurons
GSE7621	Genome U133 Plus 2.0 Array	16 PD and 9 control subjects from postmortem brains of SN
GSE83148		122 hBV patients and 6 healthy controls of liver
GSE99039		205 IPD patients and 233 healthy controls from whole blood
GSE38941		17 hBV-associated acute liver failure and 10 individual normal liver
GSE58208		22 hBV patients and 5 healthy controls from PBMC
GSE20163	GPL96[HG-U133A] Affymetrix Human	8 PD and 9 healthy controls subjects from postmortem brains of SN
GSE20164	Genome U133A Array	6 PD and 5 healthy controls subjects from SN samples

Gene Set Enrichment Analysis (GSEA) and Immune Infiltration Analysis

Gene Set Enrichment Analysis (GSEA v4.1.0)[28] was implemented to interrogate molecular pathways underlying PD and HBV pathogenesis. Immune microenvironment profiling leveraged single-sample GSEA (ssGSEA) via the GSVA package,[29] quantifying 24 reference-curated immune cell signatures within the transcriptomic datasets.[30] Differential immune cell abundance across PD/HBV cohorts versus controls was visualized through hierarchical clustering (heatmaps) and comparative distribution plots (boxplots). Significance thresholds for DEGs and pathway enrichment were established at Benjamini-Hochberg P-value < 0.05.

Biofunctional Enrichment Analysis and Weighted Correlation Network Analysis (WGCNA)

KEGG pathway and GO enrichment analyses for DEGs were conducted using the "clusterProfiler" and "GOplot" packages within the R environment. WGCNA was carried out to detect co-expressed gene modules, investigate relationships between gene networks and phenotypes of interest, and identify hub genes within these networks. A weighted adjacency matrix was constructed, and a correlation power (soft thresholding parameter) was determined to emphasize strong gene correlations while downweighting weak ones. This adjacency matrix was subsequently transformed into a topological overlap matrix (TOM) to assess gene network connectivity. The TOM aggregated adjacent genes based on the network's gene ratio and computed corresponding dissimilarity values. Average linkage hierarchical clustering, based on TOM dissimilarity measurements, was applied to group genes with similar expression patterns into modules, which were depicted by branches and distinct colors in the cluster tree, establish module relationships, and filter genes.[31]

Protein-Protein Interaction (PPI) Analysis and Screening of Hub Genes

In R software (version 4.2.0), the Venn diagram visualization of overlapping genes between PD and HBV datasets derived from WGCNA analysis was generated using the "venneuler" package. The protein-protein interaction network for 30 DEGs was constructed through the STRING database (https://cn.string-db.org/). Top-ranked hub genes were selected through maximal clique centrality (MCC) scoring implemented in the Cytohubba module of Cytoscape platform (v3.9.0). Comparative expression profiles of these key genes in PD/HBV patients versus healthy individuals were visualized using boxplot graphical representations. Subsequent validation identified six hub genes through cross-referencing PBMC data from PD cohort GSE99039 with the initial 10 candidate hub genes.

Identification of Diagnostic Genes

Diagnostic biomarker identification was conducted through receiver operating characteristic (ROC) curve evaluation employing the pROC package within the R software. Quantitative assessment of gene discriminatory capacity involved computing area under ROC curve (AUC) metrics, with a selection criterion established at AUC thresholds exceeding 0.70 for potential diagnostic biomarkers. The predictive performance of key hub genes was systematically assessed through these analytical procedures.

Anti-PD Drugs and Molecular Docking

Pharmacological agents targeting PD were acquired from the DrugBank repository (https://go.drugbank.com/). Target prediction for these compounds was executed through the Comparative Toxicogenomics Database (CTD, https://ctdbase.org/). Network

visualization of drug-target relationships was achieved using Cytoscape 3.9.0's graph theoretical framework. Toxicogenomic associations with hepatic injury were investigated by mining clinical evidence from PubMed (https://pubmed.ncbi.nlm.nih.gov/). Computational docking simulations between tolcapone and prioritized hub genes were conducted using AutoDock Vina 1.2.2,[32] with ligand structures sourced from PubChem (https://pubchem.ncbi.nlm.nih.gov/)[33] and protein conformations obtained from PDB (the Protein Data Bank, http://www.rcsb.org/). Structural preparation involved: (1) Conversion to PDBQT format with removal of crystallographic water molecules; (2) Optimization of charge states through polar hydrogen addition; (3) Establishment of 30Å³ cubic docking grids centered on protein functional domains, featuring 0.05nm grid resolution for precise spatial sampling. Comprehensive validation encompassed both molecular interaction patterns of tolcapone with hub gene products and systematic evaluation of hepatotoxic potential through integrated database analyses.

In vivo and in vitro Experimental Verification

Animal

Experimental male C57BL/6J mice (6–8 weeks, 25–30g) were procured from Cyagen Biosciences (USA) and maintained in controlled vivarium conditions (12h photoperiod, 22±2°C ambient temperature, 55±5% humidity) with ad libitum access to food and water. All experimental protocols complied with NIH guidelines for laboratory animal welfare and received ethical approval from Ethics Committee of Henan University (no. HUSOM2021-161). Following two-week environmental acclimatization, subjects underwent masked randomization into two cohorts (n=8/group): Saline (0.9% NaCl) and MPTP-induced PD model (20 mg/kg/d i.p. 1-methyl-4-phenyl-1,2,3,6-tetrahydropyridine), both administered for 15 consecutive days.[34] Terminal procedures at day 16 included: Dual-modality sampling (n=4/group): Intracardiac saline perfusion followed by 4% paraformaldehyde fixation for brain/liver histology; Hematological analysis (n=8): Retro-orbital blood collection; Molecular preservation (n=4/group): Rapid dissection of substantia nigra (SN) and hepatic tissue under cryogenic conditions, with subsequent snap-freezing in liquid nitrogen and −80°C archival storage.

Cell Culture Assay

The MN9D and AML12 cells line were purchased from Servicebio (China, Wuhan). Dopaminergic neuronal cell line MN9D, mouse liver cell line AML12, and co-cultured MN9D and AML12 cells at a 1:1 ratio were cultured in high-glucose Dulbecco's modified Eagle's medium (DMEM) (Gibco Laboratories, Grand Island, NY, USA) containing 10% fetal bovine serum (FBS), penicillin (100 units/mL), and streptomycin and incubated at 37°C in a humidified atmosphere with 5% CO_2. The culture medium was replaced every 2–3 days.

Cell Viability Testing

The MN9D and AML12 cells were treated with different concentrations of 1-methyl-4-phenylpyridinium (MPP^+) and Cys (0, 5, 10, 20, 40, 80, 160, 320, 640, and 1280 μM) for 24 h. The treated cells were then seeded in a 96-well plate with cell suspension at a density of 5×10^3/200 μL/well and incubated at 37°C in a humidified atmosphere with 5% CO_2. 10 μL of CCK-8 (catalog number: G4103, Servicebio) solution was added to each well, and the plates were further incubated for 4 h. The absorbance at 450 nm was measured using a microplate reader.

Cys, ROS, ALT, and AST Level Determination

The SN, liver, and blood samples from the saline and MPTP groups, the MPP^+-induced PD cell model, and the MPP^+-induced PD cell model were co-cultured with AML12 cells and cysteine content was detected using a cysteine colorimetric assay kit.(catalog number: E-BC-K352-M, Elabscience). reactive oxygen species (ROS) level determination in AML12 cells was performed using ROS detection kit (catalog number: G1706, Servicebio), examining different concentrations of Cys (0, 5, 10, 20, 50, 100, 200, and 300 μM) and control, MPP^+ (60 μM), Cys (30 μM), and the Cys +MPP^+ group. Blood and AML12 cell levels of ALT and AST were measured using ALT and AST assay kits (catalog numbers: SYP-M0414QX and SYP-M0413QX, UpingBio).

Total Protein Extraction and Western Blot Analysis

Cells across various treatment groups were lysed using RIPA buffer containing PMSF (product codes: G2002 and G2008; Servicebio). The lysis process involved sonication followed by centrifugation at 12,000 ×g for 10 minutes at 4°C. The

protein concentration in the resulting supernatant was quantified via a BCA assay. Subsequently, proteins were separated by SDS-PAGE and transferred onto a nitrocellulose membrane (Millipore, IPFL00010, Germany). Membranes were blocked with 5% nonfat milk in TBST for 1 hour at room temperature, then incubated overnight at 4°C with primary antibodies diluted in TBST containing 1% nonfat milk. The primary antibody panel included: α-syn, nuclear factor-κB (NF-κB p65), tumour necrosis factor α (TNFα), interleukin-1β (IL-1β), IL-6, nuclear factor-erythroid 2-related factor 2 (Nrf2), heme oxygenase 1 (HO-1), NAD(P)H quinone dehydrogenase 1 (NQO1), Caspase-3 (CASP3), NCF1, p-NCF1, selectin P ligand (SELPLG), SYK, p-SYK, GTPase-activating protein 30 (ARHGAP30) (1:1000 dilution, Affinity), tyrosine hydroxylase (TH) (1:500 dilution, Affinity), SAM and SH3 domain-containing 3 (SASH3) (Huabio, ER61213), and GAPDH (1:3000 dilution, Affinity). After primary antibody incubation, membranes were probed with HRP-conjugated secondary antibodies in 1% nonfat milk-TBST for 2 hours at room temperature. Following three 10-minute TBST washes, protein bands were visualized using chemiluminescence (Bio-Rad). Densitometric analysis of Western blot images was performed using ImageJ software.

Analysis of Immunofluorescence and Immunohistochemistry

MN9D and AML12 cells were seeded on slides, washed with PBS, and fixed with 4% paraformaldehyde at room temperature for 30 minutes. For SH-SY5Y cells cultured on chamber slides, permeabilization was achieved using 0.1% Triton X-100 for 10 minutes, followed by three PBS washes. The cells were then incubated overnight at 4°C with primary antibodies (α-syn, TH, NF-κB p65, Nrf2, and CASP3; 1:200 dilution, Affinity) diluted in 10% goat serum. After primary antibody incubation, slides were washed three times with PBS and incubated with fluorescent secondary antibodies (1:2000 dilution, Invitrogen) for 2 hours at room temperature. Nuclei were stained with DAPI for 10 minutes to visualize cell nuclei.

For immunohistochemistry, 20-μm-thick serial sections of brain and liver tissues were used. Antigen retrieval was performed by heating in 1× citrate antigen retrieval solution at 98°C for 10 minutes, followed by permeabilization with 0.1% Triton X-100 for 10 minutes. Sections were treated with hydrogen peroxide for 20 minutes in the dark to quench endogenous peroxidase activity, then blocked with 10% goat serum in PBS. Primary antibodies (TH, CASP3, and LC3A/B; all at 1:200 dilution, Affinity) were applied, and immunoreactions were visualized using a DAB kit (G1212, Servicebio). Images were captured using a Leica DMI4000B microscope (Wetzlar, Germany). Densitometric analysis of scanned immunofluorescence and immunohistochemistry images was conducted using ImageJ software to quantify signal intensity.

HE and Masson Staining

Hepatic tissue sections were stained using the HE high-definition histochemical staining kit (G1076, Servicebio) and Masson's trichrome staining kit (G1006, Servicebio) to evaluate morphological changes. The stained liver tissues were observed under a light microscope.

Statistical Analysis

Data are presented as the mean ± SEM. Comparisons between groups were performed using an unpaired Student's *t*-test and one-way ANOVA analysis of variance. ROCs were used to evaluate AUCs and the predictive abilities of diagnostic genes. All statistical tests (t-tests, ANOVA) used $P < 0.05$, with adjustments for multiple comparisons (Bonferroni) where applicable.

Results

MR Analysis

The Impact of PD on Liver Function

To investigate the impact of PD on liver function, IVs were selected for MR analysis. After a series of quality control steps, different numbers of SNPs were selected as IVs for various liver disease outcomes. The mean F-statistics for the IVs for different outcomes were all >30, indicating no evidence of weak instrument bias (Supplementary Table S2). When MR-PRESSO identified outlier SNPs during the overall test, MR analyses were re-performed after their removal, and no evidence of pleiotropic effects was found after exclusion ($P > 0.05$) (Supplementary Table S3).

Using a threshold of $P_{IVW} < 0.05$ for initial screening, the effects of PD on liver function were preliminarily assessed. The results indicated that when 33 liver function abnormalities or indicators were used as outcomes for MR analysis, PD had no significant causal effect on liver function, except for chronic hepatitis (finn-b-K11_CHRONHEP, finn-b-K11_DISLIVOTH), which showed a significant negative association. This association was further supported by two other auxiliary MR methods, all showing consistent direction and magnitude (Supplementary Table S3). Additionally, the *P*-value of Cochran's Q calculated by MR-Egger and IVW methods indicated no heterogeneity, and the intercept of the MR-Egger test suggested no horizontal pleiotropy. These results suggest that PD may reduce the incidence of hepatitis to some extent. The unusual finding that PD may reduce the incidence of chronic hepatitis piqued our interest, as previous studies have suggested that PD's regulation of distant target organs may occur through serum metabolites. Next, we examined the effects of PD on serum metabolites.

Effect of PD on Serum Metabolites

To analyze the impact of PD on serum metabolites, IVs were screened for MR analysis. The mean F-statistic values of the screened IVs were all >30, indicating no evidence of weak instrument bias. When MR-PRESSO identified outlier SNPs during the overall test, they were removed, and MR analyses were rerun. After removal, no evidence of pleiotropy was observed ($P > 0.05$) (Supplementary Table S4).

Using a threshold of $P_{IVW} < 0.05$, 14 metabolites influenced by PD were preliminarily screened (Supplementary Table S5). Among these, 7 compounds, including lysine, were found to be reduced, while the remaining 7 compounds, including eicosapentaenoate (EPA; 20:5n3), were increased (Supplementary Figure S1). These findings were corroborated by other auxiliary MR methods, which provided robust support with all algorithms showing consistent direction and magnitude (Supplementary Table S5). The *P*-value of Cochran's Q calculated by MR-Egger and IVW methods indicated no heterogeneity, and the intercept of the MR-Egger test suggested no horizontal pleiotropy. These pathways were considered potential pathways through which PD affects liver function.

Effect of Serum Metabolites on Liver Function

Having identified the types of serum metabolites influenced by PD and chronic hepatitis, the next step was to explore how PD-influenced serum metabolites affect chronic hepatitis. Effective IVs for screening target serum metabolites were selected (Supplementary Table S6) based on statistical power parameters.

Using a threshold of $P_{IVW} < 0.05$, the preliminary screening of serum metabolites affecting hepatitis revealed no significant results when finn-b-CHRONHEP_NAS was the outcome (Supplementary Table S7). However, when finn-b-K11_CHRONHEP was used as the outcome, the effect of M31453 was found to be positively associated with chronic hepatitis (Supplementary Table S7), suggesting that cysteine mediates the effect of PD on chronic hepatitis (Figure 2). However, cysteine undergoes dynamic changes in the body, and how PD specifically influences liver function through cysteine as a mediator is crucial.

Dual Role of Cysteine

Determination of Cysteine Content

The concentrations of cysteine were separately determined in the SN, liver, and serum. In the MPTP group (PD model), cysteine levels were increased compared to the saline group (Figure 3A–C). Moreover, the IC50 of MPP^+ in MN9D cells was 62.7 μM, while in AML12 cells, it was 34.38 μM. The IC50 of cysteine in MN9D cells was 52.54 μM, and in AML12 cells, it was 132.6 μM (Supplementary Figure S2A–S2D). Additionally, in the MPP^+-induced PD cell model, the MPP^+ group exhibited an increase in cysteine concentration compared to the control group (Figure 3D). When the PD cell model from MN9D was co-cultured with AML12 cells, there was an increase in cysteine concentration, although without statistical significance ($P > 0.05$) (Figure 3E).

Protective Effect of Cysteine in the PD Cell Model

Tyrosine hydroxylase (TH) and α-syn are important indicators of PD. Compared to the control group, the MPP^+ group exhibited decreased TH expression and increased α-syn expression. Different concentrations of cysteine increased TH expression and decreased α-syn protein expression compared to the MPP^+ group (Figure 3F–H). Co-localization of TH

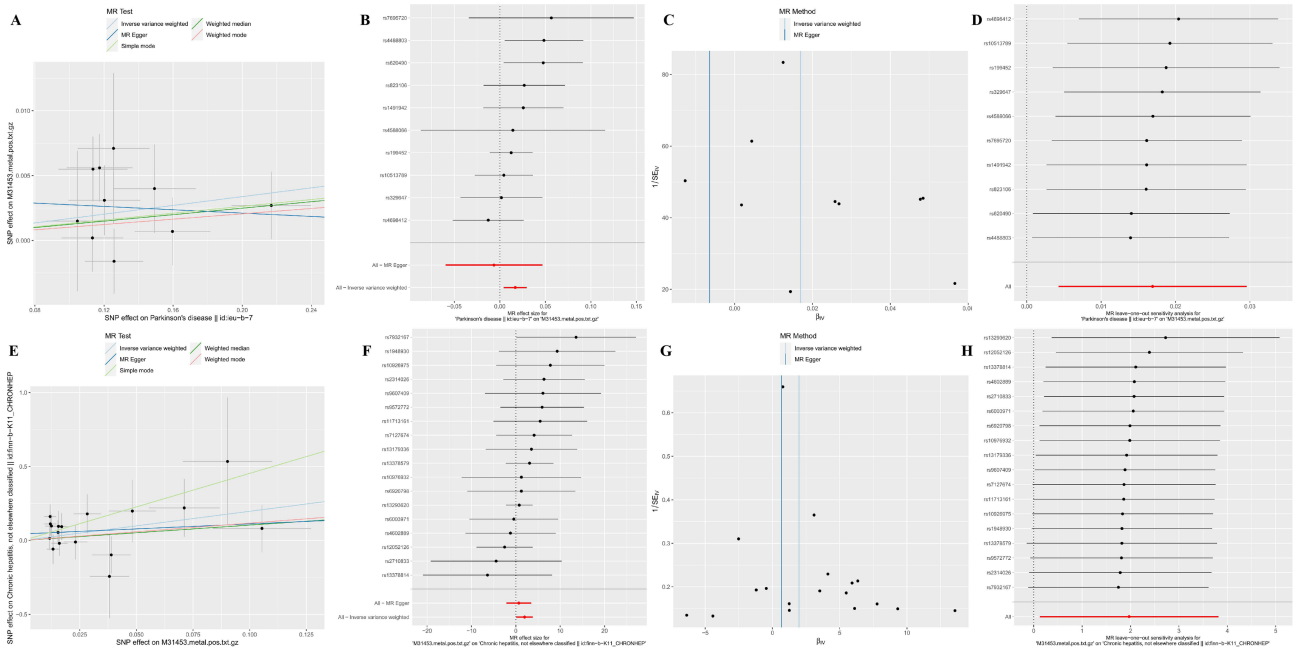

Figure 2 Cysteine mediates the effect of PD on chronic hepatitis. (**A**) Scatter plot of the MR analysis results between PD outcome and cysteine. (**B**) Effect estimates of the MR analysis results between PD outcome and cysteine. (**C**) Funnel plot of the MR analysis results between PD outcome and cysteine. (**D**) Leave-one-out sensitivity analysis results of the MR analysis results between PD outcome and cysteine. (**E**) Scatter plot of the MR analysis results between cysteine and hepatitis outcome. (**F**) Effect estimates of the MR analysis results between cysteine and hepatitis outcome. (**G**) Funnel plot of the MR analysis results between cysteine and hepatitis outcome. (**H**) Leave-one-out sensitivity analysis results of the MR analysis results between cysteine and hepatitis outcome.

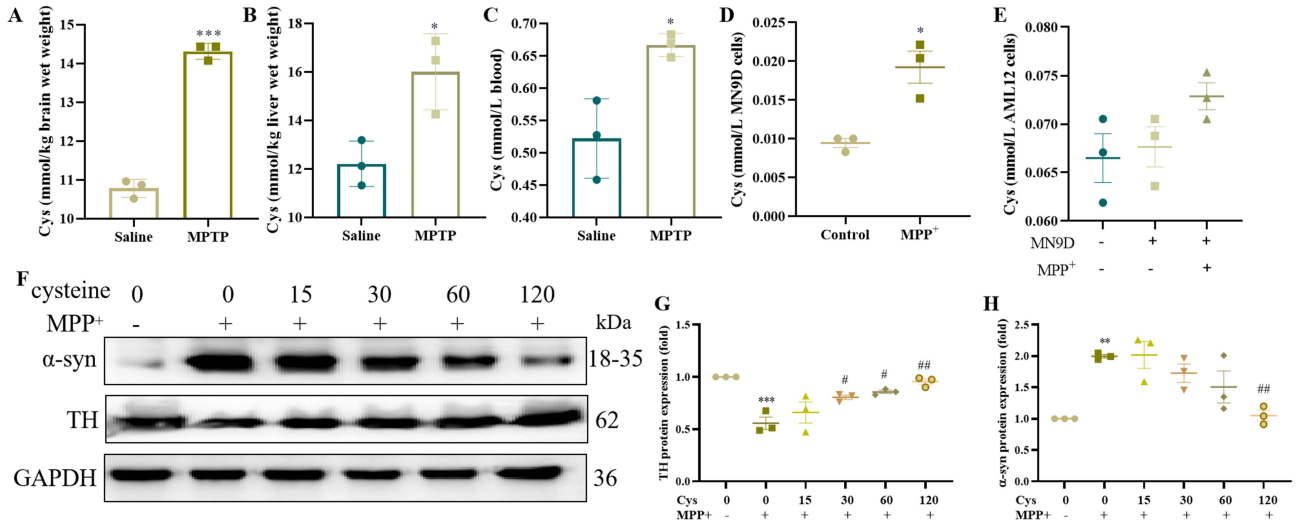

Figure 3 Determination of cysteine levels and the protective effect of cysteine in the PD cell model. (**A**) Determination of cysteine levels in the SN of the MPTP-induced PD mice model. (**B**) Determination of cysteine levels in the liver of the MPTP-induced PD mice model. (**C**) Determination of cysteine levels in the blood of the MPTP-induced PD mice model. (**D**) Determination of cysteine levels in the MPP^+-induced PD cell model. (**E**) Co-culture of MPP^+ induced MN9D PD cell model with AML12 liver cells for cysteine level determination. (**F**) Determination of TH and α-syn levels in the MPP^+-induced PD cell model following treatment with different concentrations of cysteine. (**G**) Statistical graph of TH protein. (**H**) Statistical graph of α-syn protein. Compared with the Saline or control groups, $^*P < 0.05$, $^{**}P < 0.01$, $^{***}P < 0.001$. Compared with the MPP^+ group, $\#P < 0.05$, $\#\#P < 0.01$. n = 3.

and α-syn was also investigated, and the results revealed that the MPP^+ group had decreased TH fluorescence intensity and increased α-syn fluorescence intensity. Compared to the MPP^+ group, different concentrations of cysteine increased TH fluorescence intensity but decreased α-syn fluorescence intensity in a concentration-dependent manner (Supplementary Figure S2E–S2F).

https://doi.org/10.2147/JIR.S511645

Reduced Cysteine Concentration Protects Liver Cells

Cysteine, a natural component of glutathione, contains a reactive thiol group (-SH), which provides protective effects on thiol proteases and intoxicated hepatic parenchymal cells. Low concentrations of cysteine can protect liver cells. Compared to the control group, the MPP^+ group (60 μM) exhibited increased levels of AST, ALT, proinflammatory factors (NF-κB p65, TNFα, IL-1β, IL-6), oxidative stress markers (Nrf2, HO-1, NQO1), CASP3, and ROS. After treatment with low concentrations of cysteine (30 μM), the levels of AST, ALT, inflammatory factors (NF-κB p65, TNFα, IL-1β, IL-6), CASP3, and ROS decreased compared to the MPP^+ group, while the oxidative stress markers (Nrf2, HO-1, NQO1) increased (Supplementary Figure S3). Nuclear entry of NF-κB p65 and Nrf2, as well as CASP3 fluorescence intensity, were also measured. Compared to the control group, the MPP^+ group exhibited enhanced fluorescence intensity of NF-κB p65, Nrf2, and CASP3, while after cysteine treatment, compared to the MPP^+ group, the fluorescence intensities of NF-κB p65 and CASP3 decreased while that of Nrf2 increased (Supplementary Figure S4). These findings indicate that cysteine can activate the antioxidant pathway, protecting AML12 liver cells from oxidative damage caused by ROS produced during MPP^+ metabolism.

High Levels of Cysteine Lead to Hepatocyte Damage

The extent of damage to AML12 cells following treatment with different concentrations of cysteine was subsequently assessed. Notably, as the concentration of cysteine increased, the damage to AML12 cells also increased. Compared to the control group, the ALT levels increased significantly when the cysteine concentration reached 50 μM, whereas the AST levels increased significantly at 100 μM (Figure 4A and B). Additionally, the expression of inflammatory markers (NF-κB p65, TNFα, IL-1β, IL-6) also increased with higher cysteine concentrations (Figure 4C–G). Nuclear entry of NF-κB p65 was observed, with fluorescence intensity increasing after treatment with 50 μM cysteine (Figure 4H and I). As cysteine concentration increased, the production of inflammatory factors and ROS was promoted, leading to cellular damage (Figure 4J and K). Increased levels of cysteine may promote the generation of nitrite in the body, thereby forming reactive nitrogen oxide species such as nitric oxide (NO). These reactive nitrogen oxide species can induce oxidative stress, leading to damage to cell membranes, exacerbation of inflammatory responses, and oxidative damage to intracellular proteins, nucleic acids, and other molecules, thereby affecting the normal function of cells.

Analysis of DEGs in Patients with PD or HBV

Differential Genes Obtained from the GEO Database

The expression matrices of the GSE20141 and GSE7621 datasets for PD were normalized using samples from the GPL570 platform (Supplementary Figure S5A). Principal component analysis (PCA) confirmed the repeatability of the data (Supplementary Figure S5B). Volcano plots were used to visualize DEGs, and we used an adjusted threshold of $|logFC| > 0.58$ and $P.adj < 0.05$, identifying a total of 2925 DEGs (Supplementary Figure S5C). Similarly, the expression matrix of the GSE83148 dataset for HBV was normalized using samples from the GPL570 platform (Supplementary Figure S6A). PCA and mean−variance trend verified the repeatability and lack of trend in the data (Supplementary Figure S6B and S6C). Volcano plots were used to visualize DEGs, and we used an adjusted threshold of $|logFC| > 0.58$ and $P.adj < 0.05$, identifying a total of 5204 DEGs (Supplementary Figure S6D).

GSEA and Immune Infiltration Analysis

GSEA of the PD datasets revealed that the DEGs were mainly involved in membrane trafficking, dopaminergic neurogenesis, cell cycle mitosis, mitochondrial protein import, protein folding, and autophagy (Figure 5A). In the HBV datasets, the DEGs were mainly involved in the regulation of proinflammatory and profibrotic mediators, chemokine receptors bind chemokines, metabolism of amino acids and derivatives, chemokine signaling pathway, toll-like receptor signaling pathway, and the IL8-CXCR2 pathway (Figure 5B). Heatmaps illustrating immune infiltration in the PD and HBV datasets are presented in Figure 5C and D. Compared to the normal controls, cytotoxic cells and Tcm cells were highly expressed in the PD model, whereas iDC, mast cells, and Th2 cells were lowly expressed (Figure 5E). In the HBV dataset, aDC, B cells, cytotoxic cells, iDC, Th1 cells, and Th2 cells were highly expressed, whereas eosinophils, neutrophils, Tcm, and TFH were lowly expressed (Figure 5F). There were no significant differences in immune cell expression between the PD or HBV datasets and normal controls (Supplementary Figure S7).

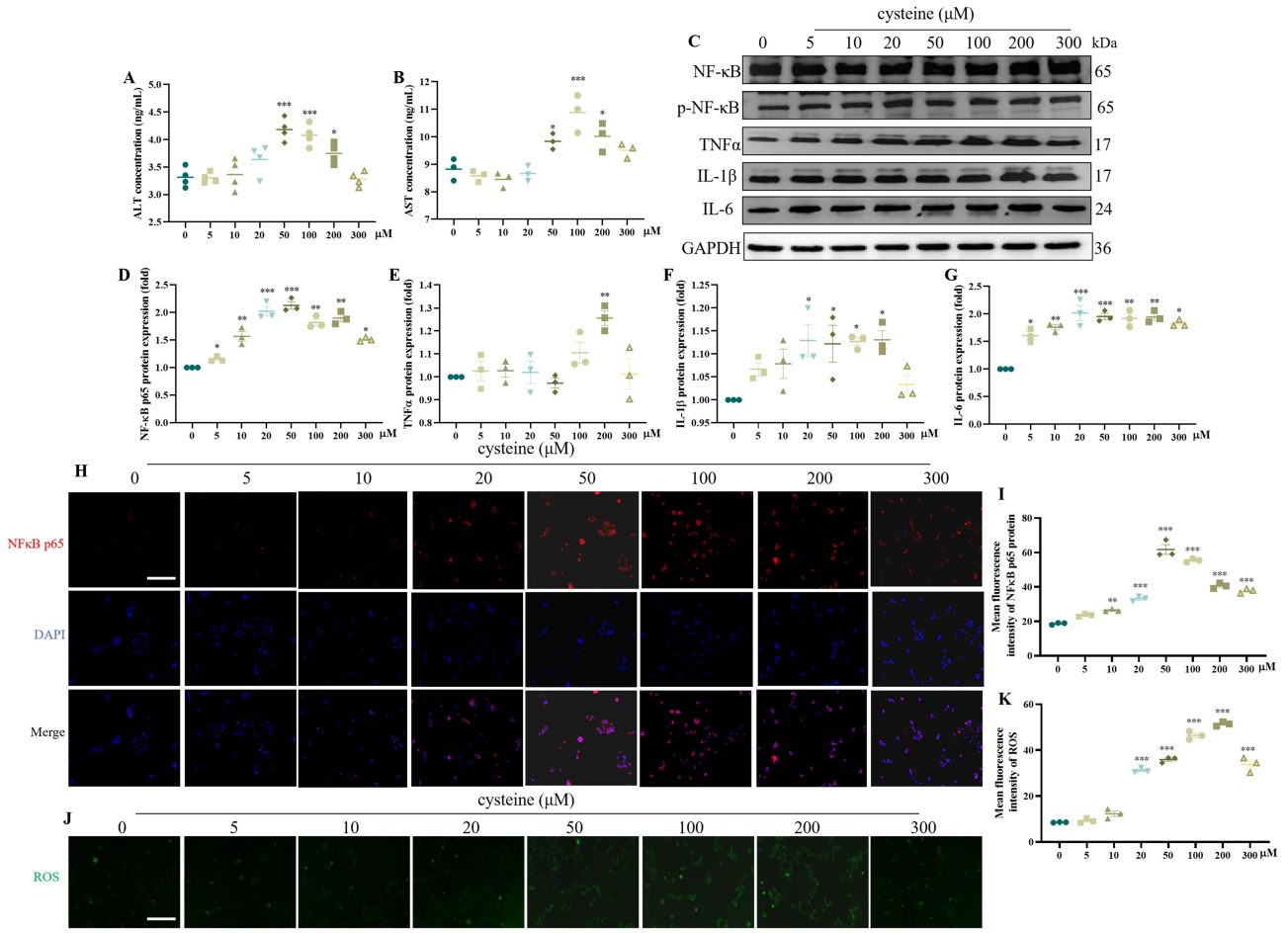

Figure 4 High concentrations of cysteine lead to hepatocyte damage and inflammation. (**A** and **B**) Determination of ALT and AST levels in AML12 cells following treatment with different concentrations of cysteine. (**C**) Western blot images showing the protein expression of NF-κB p65, TNFα, IL-1β, and IL-6. (**D**–**G**) Statistical graphs showing the protein expression of NF-κB p65, TNFα, IL-1β, and IL-6. (**H**) Determination of NF-κB p65 protein immunofluorescence intensity. (**I**) Statistical graph showing the average immunofluorescence intensity of NF-κB p65 (Scale bar, 50 μm). (**J**) Determination of ROS levels using a green fluorescence probe (Scale bar, 50 μm). (**K**) Statistical graph showing the average fluorescence intensity of ROS. Compared with the control group, **P* < 0.05, ***P* < 0.01, ****P* < 0.001. n = 3.

Biofunctional Enrichment Analysis

We identified 642 DEGs from the intersection of the PD and HBV datasets (Figure 6A). Pathway enrichment analysis of these 642 DEGs revealed involvement in several key pathways, including transcriptional misregulation in cancer, osteoclast differentiation, Chagas disease, leishmaniasis, Fc gamma R-mediated phagocytosis, legionellosis, pertussis, inflammatory bowel disease, hepatitis C, B cell receptor signaling pathway, amoebiasis, axon guidance, T cell receptor signaling pathway, and Th17 cell differentiation (Figure 6B). The enriched biological processes (BPs) mainly included axonogenesis, regulation of hemopoiesis, positive regulation of CD4-positive alpha-beta T cell activation, regulation of CD4-positive alpha-beta T cell differentiation, positive regulation of lymphocyte differentiation, dopamine biosynthetic process, and regulation of alpha-beta T cell differentiation (Figure 6C). The enriched cellular components (CC) included growth cone, site of polarized growth, actin-based cell projection, dendritic spine, neuron spine, distal axon, filopodium, transcription regulator complex, nuclear heterochromatin, and dendritic spine head (Figure 6D). The enriched molecular function (MF) included voltage-gated potassium channel activity involved in cardiac muscle cell action potential repolarization, microtubule binding, Wnt-protein binding, phosphatidylinositol-3,4-bisphosphate binding, p53 binding, tau-protein kinase activity, dynactin binding, voltage-gated potassium channel activity involved in ventricular cardiac muscle cell action potential repolarization, ATPase binding, and SH3 domain binding (Figure 6E).

https://doi.org/10.2147/JIR.S511645

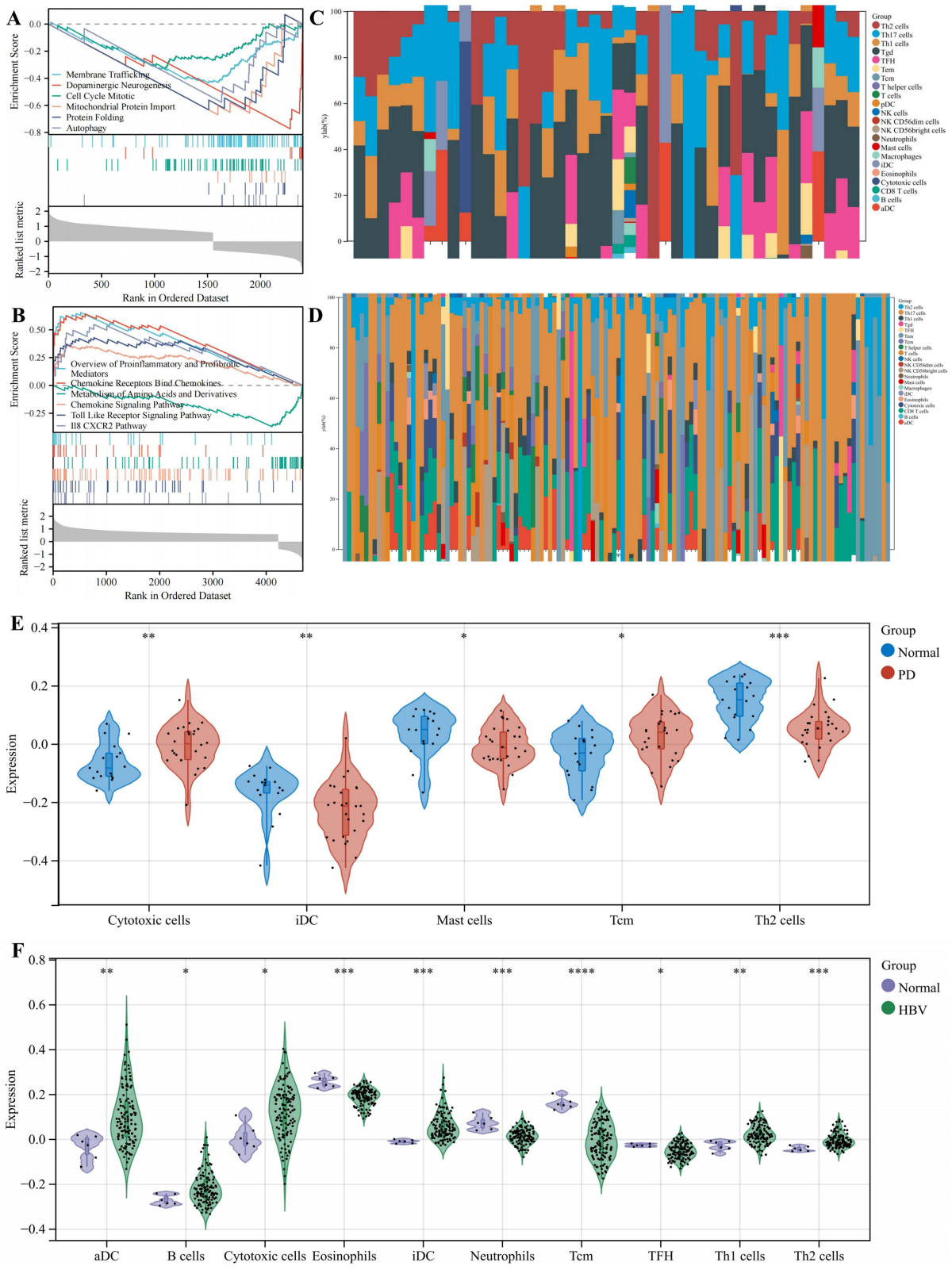

Figure 5 Immune infiltration analysis and GSEA of DEGs. (**A**) GSEA of the PD dataset. (**B**) GSEA of the HBV dataset. (**C**) Heatmap of immune infiltration analysis in the PD dataset. (**D**) Heatmap of immune infiltration analysis in the HBV dataset. (**E**) Boxplot of differentially expressed immune cells in the PD dataset. (**F**) Boxplot of differentially expressed immune cells in the HBV dataset. Compared with the normal group, **P* < 0.05, ** *P* < 0.01, ****P* < 0.001, *****P* < 0.0001.

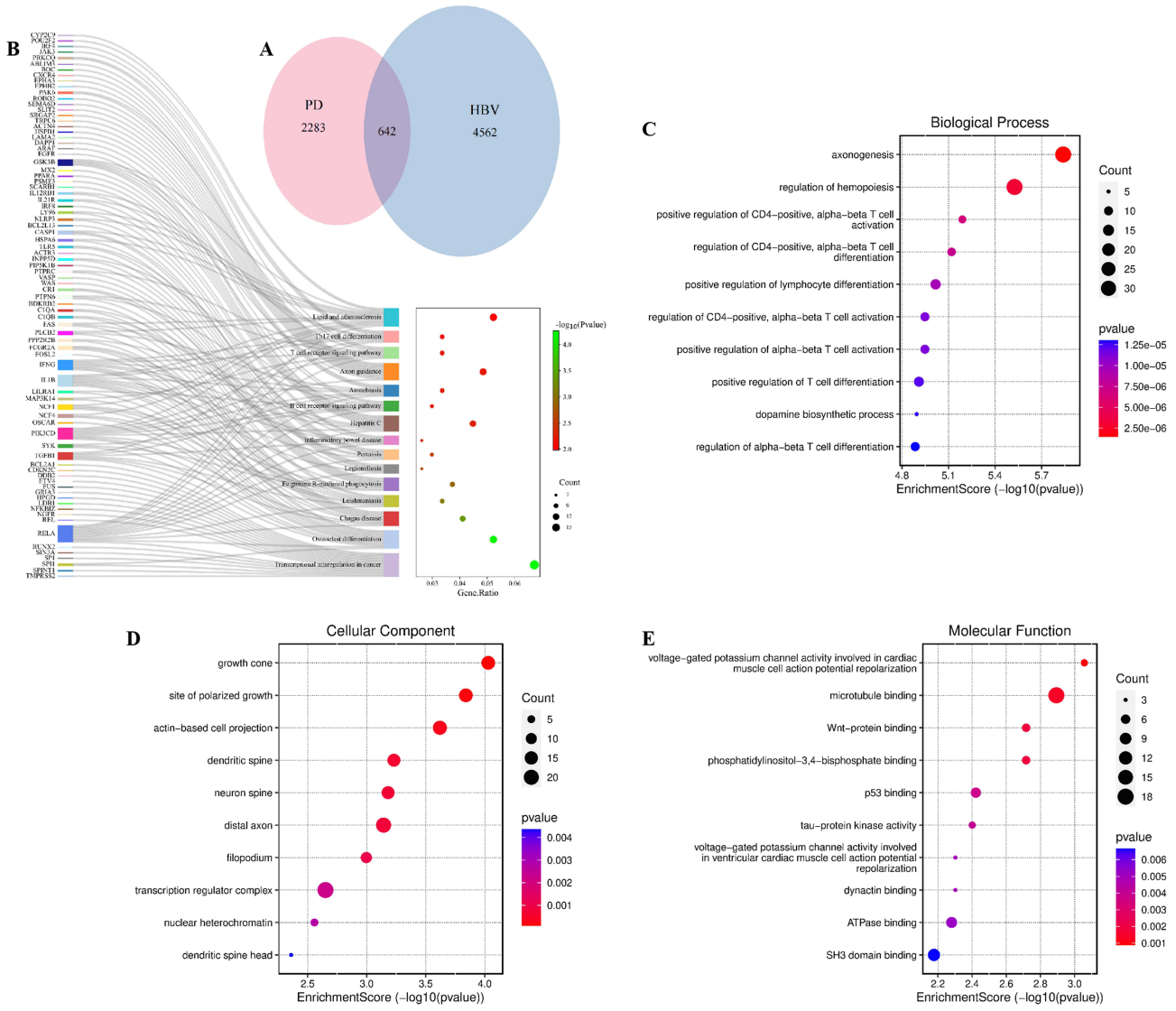

Figure 6 Signaling pathway and biofunctional enrichment analysis. (**A**) Identification of 642 common genes from the overlapping of PD and HBV datasets. (**B**) KEGG enrichment analysis. (**C**–**E**) Enrichment of BP, CC, and MF.

WGCNA Identification of Hub Genes

To comply with the scale-free network distribution principle, determining a suitable value for the adjacency matrix weight parameter (termed "power") was critical. By setting power values ranging from 1 to 30, corresponding correlation coefficients and average network connectivities were calculated. A higher correlation coefficient (up to 1) indicates closer adherence to scale-free distribution, though maintaining adequate gene connectivity was also essential—thus, the power value needed to balance sufficiently high correlation coefficients with substantial network connectivity. In this analysis, a power value of 8 was selected (Figure 7A). Using this parameter, a weighted co-expression network model was constructed, partitioning 642 genes into 4 modules. The grey module represented gene sets unassigned to any module and lacked analytical relevance (Figure 7B). Clustering heatmaps for all genes are shown in Figure 7C. Modules associated with various traits were identified using an absolute correlation coefficient threshold of ≥ 0.3 and $P < 0.05$ (Figure 7D). For the HBV dataset's WGCNA, a power value of 30 was applied, dividing 233 genes into 3 modules. Again, the grey module denoted unclassified, non-relevant gene sets (Supplementary Figure S8). Supplementary Figure S9 lists the top 50 genes ranked within each module for both PD and HBV datasets.

https://doi.org/10.2147/JIR.S511645

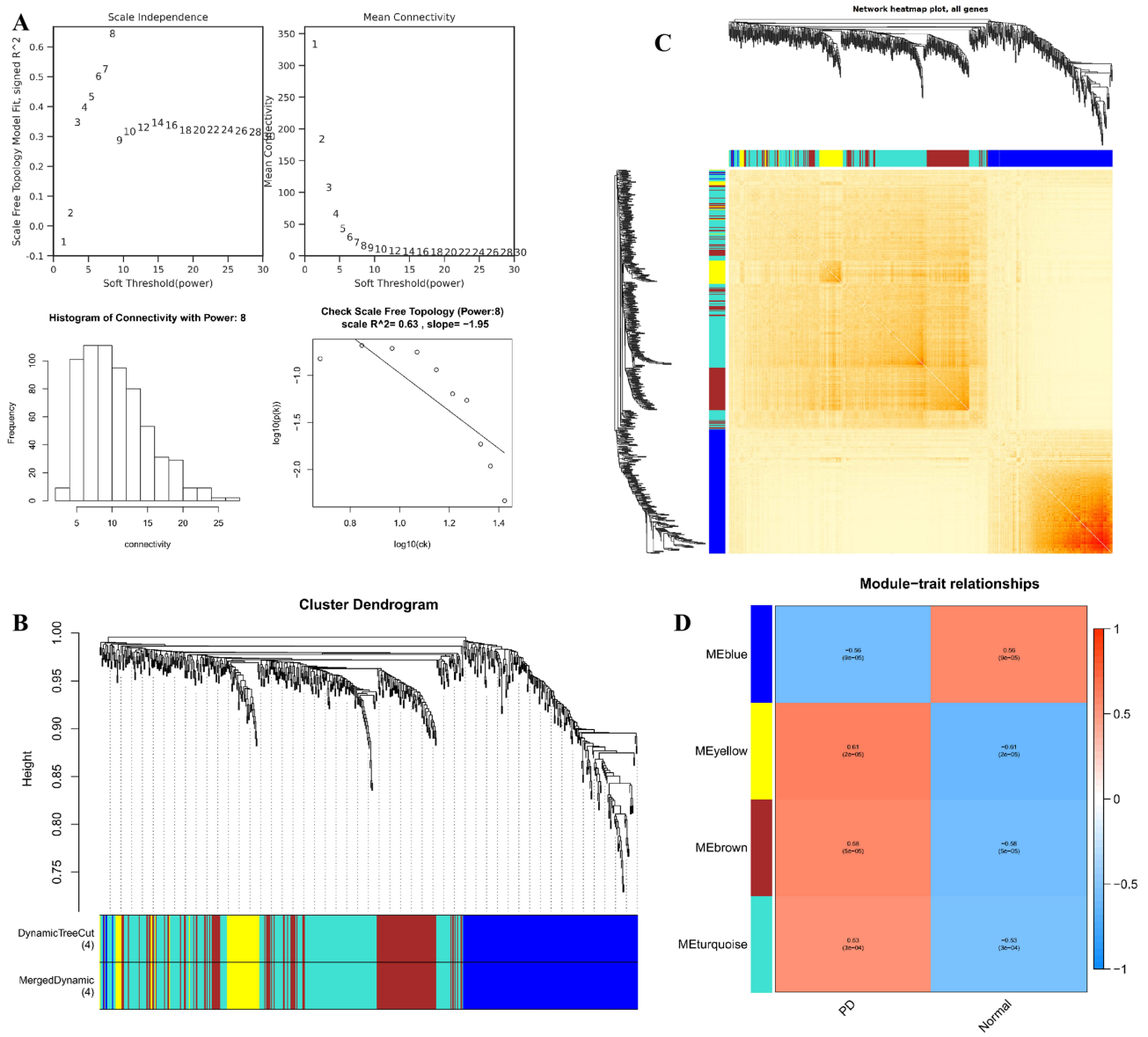

Figure 7 WGCNA of the PD dataset GSE20141 and GSE7621. (**A**) Parameters for constructing the WGCNA network. (**B**) The upper part of the figure shows the gene clustering tree constructed based on the dissTOM matrix generated using weighted correlation, whereas the lower part shows the distribution of genes in each module. Genes in the same color belong to the same module. The colors obtained using the Dynamic Tree Cut method represent modules identified by this method. Some modules were merged due to correlations, indicated as "Merged Dynamic" at the bottom, and these merged modules were used for subsequent analysis. (**C**) Heatmap of all gene clusters. (**D**) Heatmap showing the correlation between trait modules.

PPI Analysis and Hub Gene Screening

We identified 30 DEGs through the intersection of WGCNA results from PD and HBV datasets (Supplementary Figure S10A). PPI enrichment analysis revealed 29 nodes and 31 edges, with an average node degree of 2.14 and an average local clustering coefficient of 0.456. The PPI enrichment *P*-value was $<1.0\times10^{-16}$ (Supplementary Figure S10B). Using the MCC algorithm in cytohubba, 10 hub genes were identified (Supplementary Figure S10C). These hub genes were found to be highly expressed in the SN and PBMC of patients with PD, as well as in the liver and PBMC of patients with HBV (Supplementary Figure S11), suggesting that these genes play important roles in the progression of PD and HBV and are involved in multifunctional systemic metabolic regulation that is closely related to disease progression. Their biological functions are listed in Table 2. Furthermore, the hub genes were validated using the PD PBMC GSE99039 dataset (*P*.adj < 0.05), resulting in 6 hub genes: NCF1 NCF4, SELPLG, SASH3, SYK, and ARHGAP30 (Supplementary Figure S10D).

Table 2 Biological Functions of Hub Genes

Gene	Biological function
ARHGAP30	ARHGAP30 is a member of Rho GTPase-activating proteins (RhoGAPs), which can enhance the intrinsic hydrolysis of GTP and act as a negative regulator of Rho GTPases. ARHGAP30 is a RhoA- and Rac1-specific Rho GAP, involved in the regulation of cytoskeleton organization and cell adhesion. ARHGAP30 is a key regulator of p53 acetylation.
CASP1	Caspase-1 (CASP1) participates in signaling pathways associated with cell apoptosis, necrosis, and inflammation, regulating the expression of inflammatory cytokines IL-1β and IL-18, as well as activating inflammasomes. It plays a crucial role in cellular immunity and initiates pyroptosis through Gasdermin-D (GSDMD), with significant implications in cancer, aging, and cardiovascular diseases.
EVI2B	Ecotropic Viral Integration Site 2B (EVI2B) is a protein-coding gene It plays a crucial role in granulocyte differentiation and functionality of hematopoietic progenitor cells through the control of cell cycle progression and survival of hematopoietic progenitor cells.
IRF8	Interferon regulatory factor 8 (IRF8), originally termed interferon consensus sequence binding protein (ICSBP), is a member of the IRF transcription factor family. It specifically binds to the upstream regulatory region of type I interferon (IFN) and IFN-inducible MHC class I genes (the interferon consensus sequence (ICS). It can act both as a transcriptional activator and a repressor. It plays a negative regulatory role in cells of the immune system. It is also involved in CD8(+) dendritic cell differentiation by forming a complex with the BATF-JUNB heterodimer in immune cells, leading to recognition of AICE sequence (5'-TGAnTCA/GAAA-3'), an immune-specific regulatory element, followed by cooperative binding of BATF and IRF8 and activation of genes. IRF8 is required for the development of plasmacytoid dendritic cells (pDCs), which produce most of the type I IFN in response to viral infection. It positively regulates macroautophagy in dendritic cells and acts as a transcriptional repressor of osteoclast differentiation factors such as NFATC1 and EEIG1.
NCF1	NCF1 gene, also known as NOX2, encodes for NADPH oxidase, which regulates intracellular oxidative stress and immune responses. During oxidative stress, NADPH oxidase generates ROS, aiding cells in combating oxidative stress, protecting them from free radical damage, and maintaining cellular homeostasis. In immune responses, NADPH oxidase produces peroxides, which kill pathogens and regulate inflammatory responses. It also participates in cell signaling and maintaining intracellular calcium balance.
NCF4	NCF4 is a transcription factor belonging to the hypoxia-inducible factor (HIF) family. It plays a crucial role in regulating cellular functions under extreme conditions such as low oxygen and low pH. During cellular metabolism, NOX enzymes play a significant role in cellular redox reactions. Through a series of reactions, NOX enzymes generate the energy required by cells and release NO and water molecules into the extracellular space, participating in both intracellular and extracellular transport of substances.
SASH3	The protein encoded by this gene contains a Src homology-3 (SH3) domain and a sterile alpha motif (SAM), both of which are found in proteins involved in cell signaling. This protein may function as a signaling adapter protein in lymphocytes.
SELL	Selectin L (SELL) encodes a cell surface adhesion molecule that belongs to a family of adhesion/homing receptors. The encoded protein contains a C-type lectin-like domain, a calcium-binding epidermal growth factor-like domain, and two short complement-like repeats. The gene product is required for binding and subsequent rolling of leukocytes on endothelial cells, facilitating their migration into secondary lymphoid organs and inflammation sites.
SELPLG	SELPLG encodes a glycoprotein that functions as a high-affinity counter-receptor for the cell adhesion molecules P-, E-, and L-selectin expressed on myeloid cells and stimulates T lymphocytes. As such, this protein plays a critical role in leukocyte trafficking during inflammation by tethering leukocytes to activated platelets or endothelia-expressing selectins.
SYK	Non-receptor tyrosine kinase mediates signal transduction downstream of various transmembrane receptors, including classical immunoreceptors like the B-cell receptor (BCR). It also regulates several biological processes, including innate and adaptive immunity, cell adhesion, osteoclast maturation, platelet activation, and vascular development. Upon stimulation by fungal proteins, CLEC7A and SYK activate immune cells, inducing the production of ROS. Additionally, SYK activates the inflammasome- and NF-κB-mediated transcription of chemokines and cytokines in response to pathogens. It also regulates neutrophil degranulation and phagocytosis through activation of the MAPK signaling cascade and mediates the activation of dendritic cells by cell necrosis stimuli. SYK is also involved in mast cell activation and IL-3-mediated signaling pathways in basophils. Furthermore, SYK functions downstream of receptors mediating cell adhesion.

Single-Cell Type Analysis

Clustering analysis of gene cell types in the brain revealed that the genes were distributed across various clusters corresponding to excitatory neurons (c-0—c-11, c-13, c-16, c-18—c-20, c-22, c-24, c-27, c-29, c-31—c-34, c-36, c-39, c-40, c-44), oligodendrocytes (c-12, c-37), inhibitory neurons (c-14, c-15, c-17, c-21, c-23, c-25, c-26, c-28, c-30, c-38, c-41), astrocytes (c-35), oligodendrocyte precursor cells (c-42), and microglial cells (c-43). These genes are primarily expressed in microglial cells (Figure 8A). Studies have suggested that damage and overactivation of microglial cells near

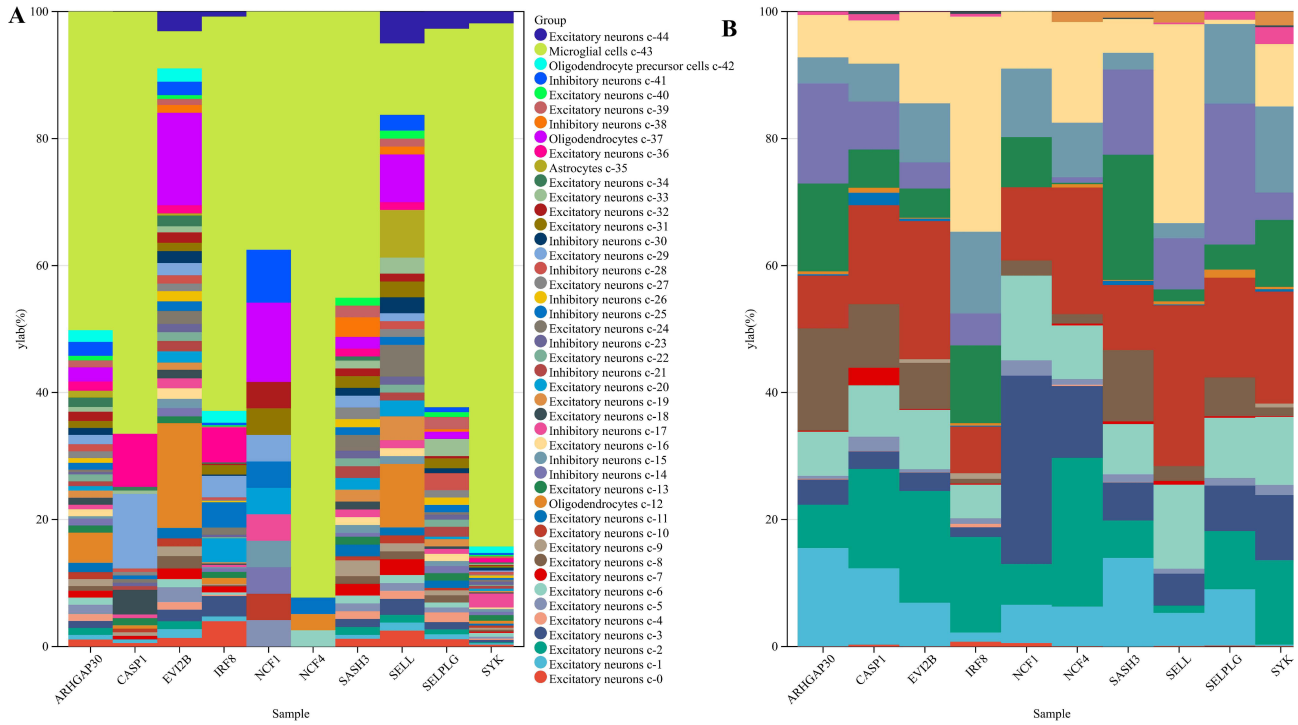

Figure 8 Single-cell type analysis of hub genes in (**A**) brain and (**B**) liver.

the risk areas within the basal ganglia and SN, trigger oxidative stress, mitochondrial autophagy and dysfunction, α-syn accumulation, and the release of pro-inflammatory cytokines. The neuronal damage mediated by these injurious factors further exacerbates microglial cell activation, further contributing to the pathological progression of PD.[35,36]

In the liver, gene cell type clustering analysis revealed distribution across various clusters corresponding to hepatocytes (c-0, c-4, c-9, c-12, c-18), T cells (c-1, c-8, c-13, c-14), macrophages (c-2, c-15), plasma cells (c-3), endothelial cells (c-5), Kupffer cells (c-6, c-10), smooth muscle cells (c-7), fibroblasts (c-11), B cells (c-16), cholangiocytes (c-17), and erythroid cells (c-19) (Figure 8B). Notably, certain genes exhibit predominant expression in specific cell types: ARHGAP30, SELPLG, and SASH3 in T cells; CASP1 and NCF4 in macrophages; EVI2B and SYK in Kupffer cells; IRF8 and SELL in B cells; and NCF1 in plasma cells. These cell types play crucial roles in immune responses and antibody production within the liver, thereby maintaining its immune defense function.

Prognostic Analysis

ROC curves were used to evaluate the diagnostic value of 6 hub genes in PD and HBV. In the SN of patients with PD, the AUC values were determined as follows: ARHGAP30 (AUC = 0.719), CASP1 (AUC = 0.735 and 0.648), EVI2B (AUC = 0.692 and 0.852), IRF8 (AUC = 0.781 and 0.597), NCF1 (AUC = 0.735 and 0.673), NCF4 (AUC = 0.765 and 0.735), SASH3 (AUC = 0.749 and 0.796), SELL (AUC = 0.667 and 0.607), SELPLG (AUC = 0.749 and 0.745), and SYK (AUC = 0.713 and 0.602) (Figure 9A and B). In the liver of patients with HBV, the AUCs were ARHGAP30 (AUC = 0.895 and 1.000), CASP1 (AUC = 0.891 and 1.000), EVI2B (AUC = 0.836 and 1.000), IRF8 (AUC = 0.939 and 0.982), NCF1 (AUC = 0.939 and 1.000), NCF4 (AUC = 0.970 and 1.000), SASH3 (AUC = 0.992 and 1.000), SELL (AUC =0.906 and 0.971), SELPLG (AUC =0.964 and 1.000), and SYK (AUC =0.945 and 1.000) (Figure 9C and D). Furthermore, validation using PBMC datasets from patients with PD or HBV revealed that these genes had high diagnostic value (AUC > 0.483) (Figure 9E and F), indicating that these genes may serve as potential targets for the diagnosis of patients with PD or HBV.

Anti-PD Drugs

Through a search of the DrugBank database, we identified 34 drugs with potential therapeutic effects in PD. Their pharmacological actions and mechanisms are detailed in Supplementary Table S8. The therapeutic targets of these 34

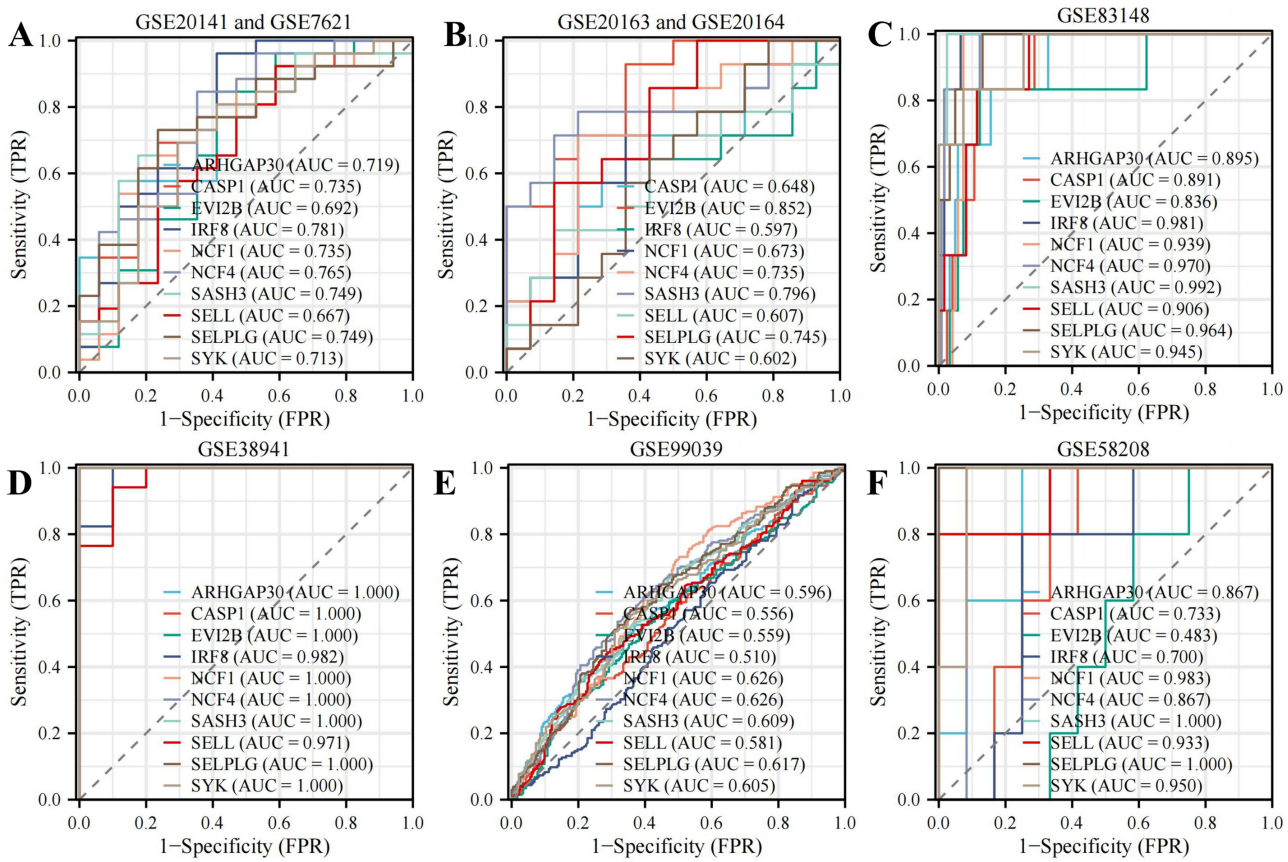

Figure 9 Diagnostic value of hub genes. (**A**) PD brain SN datasets GSE20141 and GSE7621, from the GPL570 platform, including 26 patients with PD and 17 healthy controls. (**B**) PD brain SN datasets GSE20163 and GSE20164, from the GPL96 platform, including 14 patients with PD and 14 healthy controls. (**C**) HBV liver tissue dataset GSE83148, from the GPL570 platform, including 122 patients with HBV and 6 healthy controls. (**D**) HBV liver tissue dataset GSE38941, from the GPL570 platform, including 17 patients with HBV and 10 healthy controls. (**E**) PD PBMC dataset GSE99039, from the GPL570 platform, including 233 healthy controls and 205 patients with PD. (**F**) HBV PBMC dataset GSE58208, from the GPL570 platform, including 12 patients with HBV and 5 healthy controls.

drugs primarily include inflammatory factors (IL1α, IL1β, IL24, TNF, RELA, Fos, and secretary leukocyte protease inhibitor (SLPI)), chemokines (C-X-C Motif Chemokine Ligand 8 (CXCL8)), apoptosis-related factors (BAX, CASP3, CASP9, and BCL2), hepatic drug-metabolizing enzymes (cytochrome P450 family 1 subfamily A member 1 (CYP1A1) and CYP1A2), oxidative stress regulators (Nrf2 and catalase (CAT)), monoamine oxidases (monoamine oxidase A (MAOA) and MAOB), neurotrophic factors, dopamine receptors D1 (DRD1) and DRD2), transporter protein families (solute carrier family 22 member 2 (SLC22A2) and SLC7A11), prolactin (PRL), potassium voltage-gated channel subfamily H member 2 (KCNH2), catechol-O-methyltransferase (COMT), prostaglandin-endoperoxide synthase 2 (PTGS2), α-syn, mitogen-activated protein kinase (MAPK), and bone morphogenetic protein 6 (BMP6) (Figure 10). Additionally, it was found that tolcapone, one of the 34 drugs, could induce liver injury (Supplementary Table S9), prompting further experimental validation regarding whether tolcapone indeed causes liver damage.

Molecular Docking

The binding poses and interactions of tolcapone with hub genes were obtained using Autodock Vina v.1.2.2, which generated binding energies for each interaction. The results showed that tolcapone binds to hub genes via hydrogen bonds and strong electrostatic interactions. The binding energies of tolcapone with NCF1, NCF4, SELPLG, SASH3, SYK, and ARHGAP30 are −8.0 kcal/mol, −7.6 kcal/mol, −5.9 kcal/mol, −6.8 kcal/mol, −9.3 kcal/mol, and −6.0 kcal/mol, respectively (Figure 11). The binding energies and corresponding amino acid sites are detailed in Table 3.

https://doi.org/10.2147/JIR.S511645

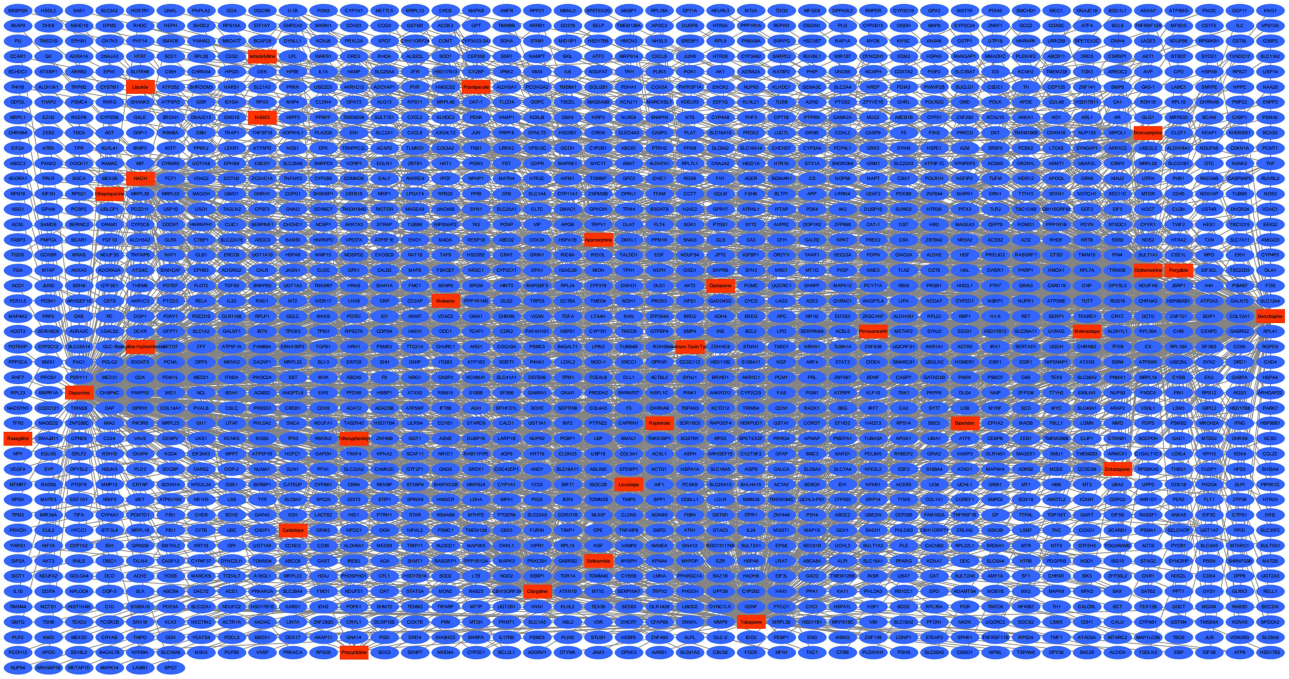

Figure 10 The drug-target network. Red represents anti-PD drugs, and blue represents drug-related targets.

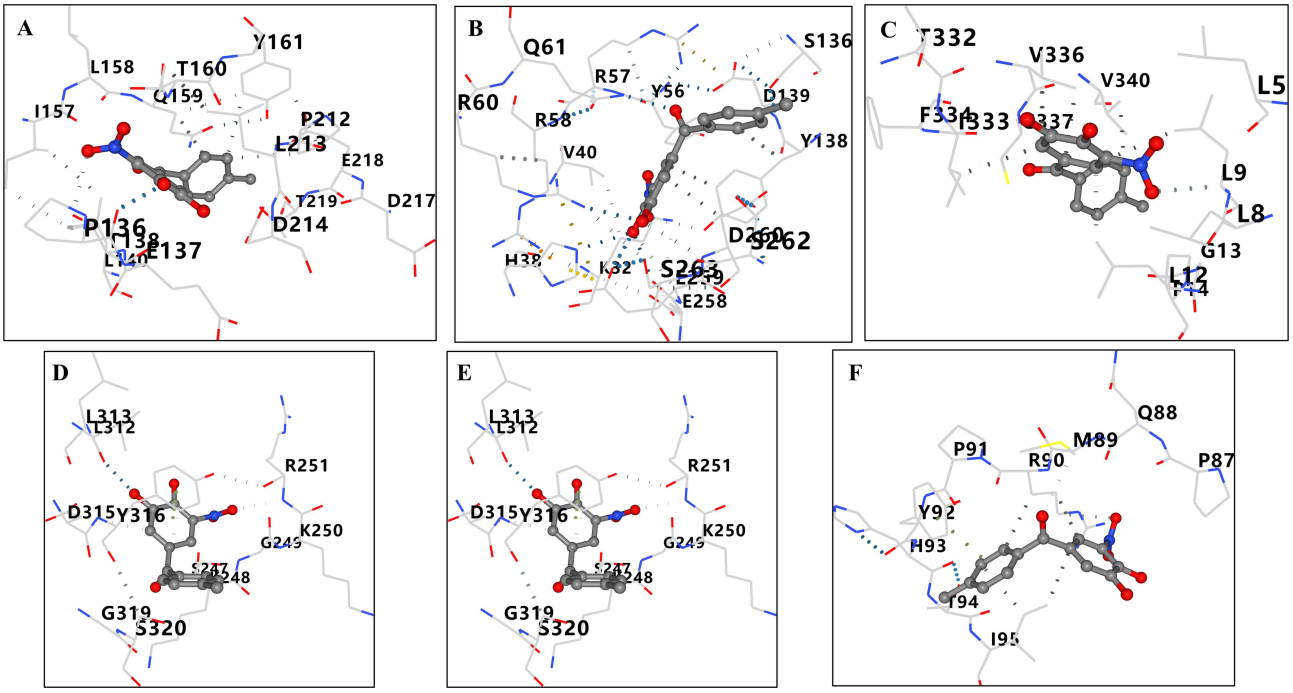

Figure 11 Molecular docking of tolcapone with various hub genes (**A**) NCF1 (AF-P14598-F1), (**B**) NCF4 (AF-Q15080-F1), (**C**) SELPLG (AF-Q14242-F1), (**D**) SASH3 (AF-O75995-F1), (**E**) SYK (AF-Q15046-F1), and (**F**) ARHGAP30 (AF-A0A0A0MRJ8-F1).

Effect of Tolcapone on Hub Genes and Its Impact on Liver Damage

First, the effects of tolcapone on the hub genes were assessed. Compared to the control group, in the MPP^+-induced PD cell model, the expression levels of NCF1, SELPLG, SASH3, SYK, and ARHGAP30 were elevated. Treatment with Tolcapone resulted in a concentration-dependent decrease in the expression of these proteins (Figure 12A–F). Additionally, tolcapone led

Table 3 Binding Energies and Corresponding Amino Acid Sites

Protein	Binding Energy	Amino Acid Sites
NCF1	−8.0 kcal/mol	Chain A: GLU15 GLU88 ASP130 LYS135 PRO136 GLU137 THR138 TYR139 LEU140 MET141 ILE157 LEU158 GLN159 THR160 TYR161 VAL182 GLU184 LYS188 PRO212 LEU213 ASP214 ASP217 GLU218 THR219 GLU220
NCF4	−7.6 kcal/mol	Chain A: LYS32 hIS38 VAL40 TYR56 ARG57 ARG58 ARG60 GLN61 ALA64 LEU65 ASP128 ILE131 PHE132 PHE133 TYR134 SER136 PRO137 TYR138 ASP139 GLU258 GLU259 ASP260 SER262 SER263
SELPLG	−5.9 kcal/mol	Chain A: LEU5 LEU6 LEU8 LEU9 ILE10 LEU12 GLY13 PRO14 GLY15 SER17 ALA328 LEU329 THR332 ILE333 PHE334 VAL336 CYS337 VAL339 VAL340 LEU341 VAL343 ARG344 ARG347
SASH3	−6.8 kcal/mol	Chain A: ARG244 GLN246 SER247 LYS248 GLY249 LYS250 ARG251 PRO252 PRO254 GLU259 LEU260 GLU262 ARG263 ILE264 ALA309 LEU312 LEU313 ASP315 TYR316 GLY319 SER320
SYK	−9.3 kcal/mol	Chain A: GLY277 ALA278 VAL279 ILE298 ALA299 PRO300 GLU301 GLN321 ARG323 GLU325 THR330 hIS331 ASN332 GLU334 PHE335 THR336 THR337 CYS338 GLU339 TYR341 ARG485 GLU487 GLU494 ILE495 CYS496 ASN497 TYR499 TRP547 GLY548 MET549 GLY550 ILE551 ASP552 ARG553 VAL554 ILE564
ARHGAP30	−6.0 kcal/mol	Chain A: PRO87 GLN88 MET89 ARG90 PRO91 TYR92 hIS93 THR94 ILE95 ILE96

to increased levels of ALT and AST in AML12 liver cells in a concentration-dependent manner (Figure 12G and H), indicating tolcapone-induced liver injury. Compared to the control group, MPP^+ treatment resulted in elevated concentrations of AST and ALT. Upon administration of tolcapone at a concentration of 100 μM, significant increases in AST and ALT concentrations were observed compared to the MPP^+ group (Figure 12I and J). These findings suggest that both the PD modeling agent and tolcapone can induce liver injury, warranting further validation in a PD mouse model.

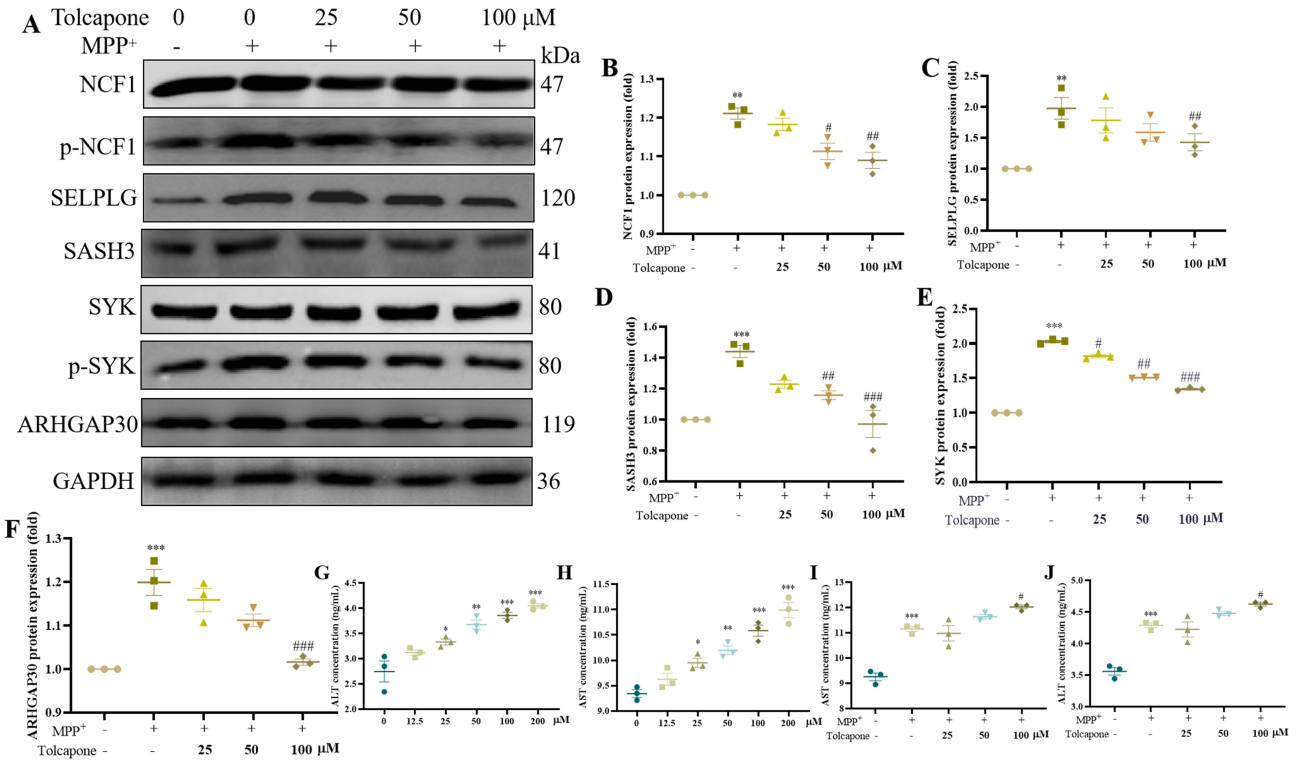

Figure 12 Effect of tolcapone on hub genes and hepatocellular damage. (**A**) Determination of NCF1, SELPLG, SASH3, SYK, and ARHGAP30 protein expression levels in MPP^+-induced PD cell model treated with different concentrations of Tolcapone. (**B**–**F**) Statistical graphs showing the expression levels of NCF1, SELPLG, SASH3, SYK, and ARHGAP30 proteins. (**G** and **H**) Determination of ALT and AST concentrations in AML12 liver cells treated with different concentrations of tolcapone. (**I** and **J**) Determination of AST and ALT concentrations in MPP^+-induced AML12 liver cells treated with different concentrations of tolcapone. Compared with the control group, *$P < 0.05$, **$P < 0.01$, ***$P < 0.001$. Compared with the MPP^+ group, #$P < 0.05$, ##$P < 0.01$, ###$P < 0.001$. n = 3.

https://doi.org/10.2147/JIR.S511645

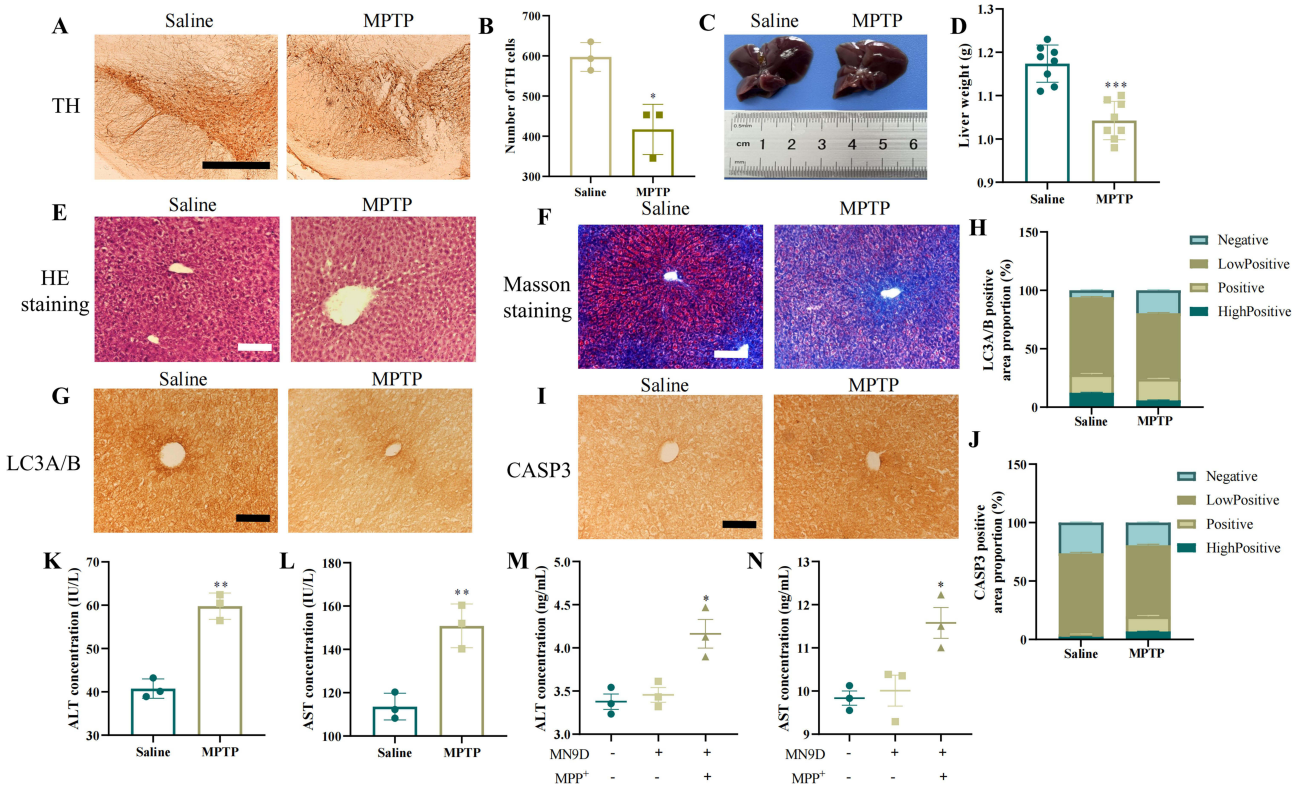

Figure 13 Liver damage in the MPTP-induced PD mice model. (**A**) Determination of TH content in the MPTP-induced PD mice model. (**B**) Statistical graph of TH cell count. (**C**) Anatomy of the liver in the MPTP-induced PD mice model. (**D**) Statistical graph of liver weight. (**E**) Analysis of liver HE staining in the MPTP-induced PD mice model. (**F**) Analysis of liver Masson staining in the MPTP-induced PD mice model. (**G**) Immunohistochemical staining of LC3A/B in liver. (**H**) Statistical graph of LC3A/B-positive ratio. (**I**) Immunohistochemical staining of CASP3 in liver. (**J**) Statistical graph of CASP3-positive ratio. (**K** and **L**) Determination of ALT and AST levels in the blood of MPTP-induced PD mice model. (**M** and **N**) Co-culture of MPP^+-induced MN9D PD cell model with AML12 liver cells to determine ALT and AST levels. Compared with the Saline or control group, $^*P < 0.05$, $^{**}P < 0.01$, $^{***}P < 0.001$. n=3.

Compared to the saline group, MPTP led to a significant decrease in TH levels (Figure 13A and B). MPTP treatment also resulted in a significant decrease in liver weight (Figure 13C and D). The liver histology of mice in the saline group revealed intact lobular structure, clear outlines of hepatic parenchymal cells, evenly distributed nuclei, and an orderly arrangement of liver cells. In the MPTP group, extensive diffuse degeneration and necrosis were observed near the hepatic portal vein, with disordered arrangement of liver cells at the edges, most of which were in a swollen state, along with inflammatory cell infiltration (Figure 13E). Masson staining revealed collagen fiber deposition in the hepatic portal area in the saline group. Compared to the saline group, pseudo-lobules were observed in the hepatic portal and central vein areas of mice in the MPTP group, with the formation of fibrous septa and an increase in collagen fiber deposition (Figure 13F). Immunohistochemistry revealed decreased autophagy and increased apoptosis in the MPTP group compared to the saline group, with decreased levels of LC3 high positive and low positive and increased levels of Negative; increased levels of CASP3 high Positive and Low Positive and decreased level of Negative (Figure 13G–J, Table 4). Compared to the saline group, the MPTP group exhibited an increase in ALT and AST concentrations

Table 4 Proportion of LC3A/B and CASP3 Positive Degree

Protein	Group	High Positive	Positive	Low Positive	Negative
LC3A/B	Saline	12.29±0.58	15.83±0.87	66.05±0.65	5.83±0.50
	MPTP	5.82±0.32$^{(**)}$	15.59±0.53	56.25±0.65$^{(***)}$	19.54±0.73$^{(***)}$
CASP3	Saline	2.29±0.10	2.24±0.18	69.20±0.82	26.26±0.62
	MPTP	6.78±0.34$^{(**)}$	12.93±0.90$^{(**)}$	60.84±0.93$^{(**)}$	19.45±0.48$^{(**)}$

Notes: Compared with the Saline group, $^{**}P < 0.01$, $^{***}P < 0.001$.

(Figure 13K and L). After co-culturing MN9D and AML12 cells, the ALT and AST concentrations increased in the MPP^+-induced PD cell model of AML12 liver cells compared to the control group (Figure 13M and N).

Discussion

Through MR analysis, we found that PD does not have a significant causal impact on most liver diseases. However, a negative association was found with chronic hepatitis (finn-b-K11_CHRONHEP, finn-b-K11_DISLIVOTH). We speculate that the influence of PD on the liver is dynamic and complex, and the current data is still incomplete. Nevertheless, experimental validation has confirmed some effects of PD on the liver. Further analysis of serum metabolites revealed a positive causal effect between PD and cysteine, a serum metabolite associated with chronic hepatitis (finn-b-K11_CHRONHEP). This finding suggests that PD may influence the development of chronic hepatitis by modulating cysteine levels. The experimental study further investigates the role of cysteine in PD cell models. Specifically, moderate levels of cysteine have protective antioxidant effects on liver cells, while high concentrations of cysteine may lead to increased oxidative stress and damage to liver cells. Therefore, controlling the concentration of cysteine is crucial for maintaining the health and function of liver cells. Additionally, comprehensive bioinformatics analysis revealed the biological functions and single-cell localization information of common genes in PD and HBV diseases. Furthermore, the study confirmed that the use of tolcapone in PD treatment can exacerbate liver damage.

The liver is the largest digestive organ in the human body and has a strong ability to metabolize foreign substances. It is the main organ responsible for maintaining systemic metabolic homeostasis.[37] Liver injury is often accompanied by the release of certain metabolites related to the occurrence of neurodegenerative disorders.[38] Currently, there is increasing evidence to suggest that PD is not only a neurodegenerative disorder but also a systemic disease, implying that the pathological changes in PD also affect peripheral organs outside the brain. Therefore, studying other peripheral tissues may provide new insights into the pathogenesis of PD. There is growing clinical evidence suggesting a connection between the CNS and liver metabolism, especially in patients with PD.[39,40] Controlling further liver damage in patients with PD is of great significance for maintaining their systemic homeostasis and avoiding potential risks associated with medication. This study demonstrates that PD can affect liver function through serum metabolites. Specifically, disruptions in cysteine metabolism were detected in the SN, liver, and blood of the PD animal model, indicating the importance of cysteine in the pathogenesis of PD. In the MPTP-induced PD mice model, increased levels of cysteine were observed in the SN, liver, and blood of the mice. Decreased cysteine concentration in the MPP^+-induced PD cell model led to reduced α-syn aggregation and increased TH expression, indicating decreased cellular damage. Thus, at low concentrations, cysteine's anti-inflammatory, anti-apoptotic, and antioxidant effects protect liver cells from oxidative damage. However, high cysteine concentrations promoted inflammation and oxidative stress, resulting in excessive ROS production and liver cell damage. Therefore, cysteine levels could serve as biomarkers for detecting liver damage in patients with PD and as targets for future therapeutic interventions.

Furthermore, shared hub genes between PD and HBV were identified, and several studies have reported the functions of these genes. For example, the NCF1 and NCF4 genes play an important role in immune responses. They are involved in the respiratory burst generation during neutrophil activation, providing cells with redox capabilities to kill bacteria and regulate immune activity during inflammation.[41] Variations in these genes may influence neutrophil function and inflammatory responses in both PD and HBV infections. SELPLG plays an important role in inflammatory responses and the adhesion of immune cells. SELPLG binds to P-selectin on the surface of endothelial cells, facilitating the migration and infiltration of leukocytes and immune cells.[42] In PD and HBV, variations in the SELPLG gene may regulate leukocyte adhesion and the inflammatory response. The protein encoded by the SASH3 gene contains sterile alpha motif (SAM) and Src homology 3 (SH3) domains, which play important roles in signal transduction and protein interactions. The SAM domain may be involved in protein interactions and signal transduction, whereas the SH3 domain may mediate the binding of the protein to other domains.[43] In PD and HBV, SASH3 may regulate inflammation and immune responses by participating in signal transduction pathways. The protein encoded by the SYK gene is a tyrosine kinase that is involved in signal transduction and immune response in B cells and macrophages. SYK plays a critical role in the signaling process, regulating the activation of immune cells and inflammatory responses.[44] In PD and HBV, variations in the SYK gene may affect the activation of immune cells and inflammatory response. The ARHGAP30 gene

is involved in the regulation of the cytoskeleton and cell migration.[45] ARHGAP30 may affect the pathogenesis of PD and HBV by regulating cell migration and inflammatory response. In summary, the shared genes between PD and HBV may impact the function of neutrophils and inflammatory responses, regulate leukocyte adhesion and inflammatory responses, as well as participate in signal transduction and immune responses.[46–48] The innovation of our research lies in identifying potential genes that could be used as therapeutic targets.

This study demonstrated that while drugs effective for treating PD show promise, they may also target pathways leading to liver damage. Previous studies have demonstrated that tolcapone can cause mitochondrial uncoupling via oxidative phosphorylation, resulting in damage to liver cell energy production. In Phase III clinical trials for PD treatment, 1% of patients taking 100 mg of tolcapone three times daily had serum ALT levels increase above three times the upper limit of normal. This percentage increased to 3% among those taking 200 mg three times daily.[49,50] These observations confirm the hepatotoxic potential of the drug. In our study, treating PD cell models with tolcapone resulted in decreased expression levels of NCF1, NCF4, SELPLG, SASH3, SYK, and ARHGAP30, along with other classical treatment indicators, compared to MPP^+ treatment. However, as the concentration of tolcapone increased, the levels of AST and ALT also increased. In conclusion, our results indicate that tolcapone treatment potentially regulates the expression of PD-related genes. However, it is important to note that tolcapone treatment can also cause liver damage. Therefore, when using tolcapone or similar drugs for PD treatment, close monitoring of patients' liver function indicators should be considered, and appropriate treatment and management measures should be taken to balance the therapeutic effects with the adverse effects.[51,52] In neurotoxin-induced models of PD, neurotoxins such as 6-hydroxydopamine (6-OHDA), MPTP, MPP^+, paraquat, and rotenone may directly damage the liver through mechanisms such as oxidative stress, inflammation, and mitochondrial dysfunction.[53–55] We also observed an increase in AST and ALT levels in the MPP^+-induced liver cells. While lower concentrations of tolcapone were found to decrease AST and ALT levels, higher concentrations led to increased levels of these enzymes. Similarly, in MPTP-induced PD animal models, an increase in AST and ALT levels was observed, along with reduced liver autophagy and increased apoptosis.

While our study demonstrates a causal link between PD and liver dysfunction mediated by cysteine and shared immune pathways, alternative explanations warrant consideration. First, pharmacological interventions for PD (eg, levodopa) may independently alter liver metabolism, though our experimental models controlled for this via MPTP/MPP^+ toxicity. Second, lifestyle factors (eg, diet, alcohol) and comorbidities (eg, metabolic syndrome) could confound clinical associations; future MR analyses should incorporate these covariates where feasible. Lastly, gene-environment interactions (eg, toxin exposure) may modulate the PD-liver axis, emphasizing the need for integrated omics and environmental data in subsequent work. Prospective studies should track liver function in PD patients stratified by medication use, dietary habits, and genetic risk profiles to disentangle confounding effects. Additionally, organoid models co-culturing neuronal and hepatic cells could elucidate bidirectional brain-liver communication pathways.

The identification of cysteine as a biomarker and hub genes (eg, NCF1) as therapeutic targets opens avenues for personalized medicine in PD management. The integration of MR, transcriptomics, and experimental validation mitigates biases inherent to any single approach. Although this study proposes several new suggestions, it still has some limitations. The research data is mainly based on cell models and animal experiments and further validation is needed in humans. More in-depth exploration is needed to investigate the mechanisms and interrelationships between PD and liver metabolism. More in-depth research and clinical observations are needed to understand the mechanisms of liver damage and the clinical impact of tolcapone treatment. Future treatment strategies need to focus on maximizing the therapeutic effectiveness of PD medications while reducing their hepatotoxic effects. More biological and bioinformatics analyses should be conducted to reveal the deeper connections between PD and liver metabolic homeostasis. Prospective clinical cohorts are needed to validate the temporal dynamics of PD-associated liver damage and assess causality beyond genetic proxies. These limitations and future research plans will contribute to further improving the understanding of the relationship between PD and liver diseases and provide important guidance and evidence for future treatments and clinical practices.

Conclusion

Research shows that PD-related brain damage does indeed have an impact on liver metabolic function. Specifically, PD-related brain damage may disrupt the concentration of homocysteine, and high levels of homocysteine may lead to liver cell damage and oxidative stress. By comparing the gene expression differences in the transcriptomes of PD and liver injury tissues, some common genes or functions that may interact across tissues were identified. For example, specific genes involved in immune and inflammatory responses (such as NCF1, NCF, and SELPLG) may lead to liver injury. The study suggests that homocysteine can serve as a biomarker for PD-related liver injury and a therapeutic target, providing important insights for future treatment strategies for PD. The study also evaluated the impact of the anti-PD drug tolcapone on liver function. It was found that besides having significant therapeutic.

Data Sharing Statement

All data and materials generated or analyzed during this study are included in this published article [and its supplementary information files].

Ethics Approval

This study was approved by the Ethics Committee of Henan University (no. HUSOM2021-161).

Author Contributions

All authors made a significant contribution to the work reported, whether that is in the conception, study design, execution, acquisition of data, analysis and interpretation, or in all these areas; took part in drafting, revising or critically reviewing the article; gave final approval of the version to be published; have agreed on the journal to which the article has been submitted; and agree to be accountable for all aspects of the work.

Funding

This study was supported partly by National Natural Science Foundation of China grant (32161143021, 81271410), Henan Province Natural Science Foundation of China (182300410313), and Henan University graduate «Talent Program» of Henan Province (SYLYC2023092).

Disclosure

The authors declare no conflicts of interest regarding the publication of this paper.

References

1. Ye H, Robak LA, Yu M, Cykowski M, Shulman JM. Genetics and pathogenesis of Parkinson's syndrome. *Annu Rev Pathol*. 2023;18:95–121. doi:10.1146/annurev-pathmechdis-031521-034145
2. Dorsey ER, Sherer T, Okun MS, Bloem BR. The emerging evidence of the Parkinson pandemic. *J Parkinson's Dis*. 2018;8(s1):S3–S8. doi:10.3233/JPD-181474
3. Popa-Wagner A, Dumitrascu DI, Capitanescu B, et al. Dietary habits, lifestyle factors and neurodegenerative diseases. *Neural Regen Res*. 2020;15(3):394–400. doi:10.4103/1673-5374.266045
4. Balestrino R, Schapira AHV. Parkinson disease. *Eur J Neurol*. 2020;27(1):27–42. doi:10.1111/ene.14108
5. Zhang J, Culp ML, Craver JG, Darley-Usmar V. Mitochondrial function and autophagy: integrating proteotoxic, redox, and metabolic stress in Parkinson's disease. *J Neurochem*. 2018;144(6):691–709. doi:10.1111/jnc.14308
6. Beraza N, Trautwein C. The gut-brain-liver axis: a new option to treat obesity and diabetes? *Hepatology*. 2008;48(3):1011–1013. doi:10.1002/hep.22478
7. Vegas-Suárez S, Simón J, Martínez-Chantar ML, Moratalla R. Metabolic diffusion in neuropathologies: the relevance of brain-liver axis. *Front Physiol*. 2022;13:864263. doi:10.3389/fphys.2022.864263
8. Zheng H, Cai A, Shu Q, et al. Tissue-specific metabolomics analysis identifies the liver as a major organ of metabolic disorders in amyloid precursor protein/presenilin 1 mice of Alzheimer's disease. *J Proteome Res*. 2019;18(3):1218–1227. doi:10.1021/acs.jproteome.8b00847
9. Bugianesi E, Moscatiello S, Ciaravella MF, Marchesini G. Insulin resistance in nonalcoholic fatty liver disease. *Curr Pharm Des*. 2010;16(17):1941–1951. doi:10.2174/138161210791208875
10. Kermanizadeh A. Preparation and utilization of a 3D human liver microtissue model for nanotoxicological assessment. *Methods Mol Biol*. 2019;1894:47–55. doi:10.1007/978-1-4939-8916-4_3
11. Petersen MC, Vatner DF, Shulman GI. Regulation of hepatic glucose metabolism in health and disease. *Nat Rev Endocrinol*. 2017;13(10):572–587. doi:10.1038/nrendo.2017.80

12. Vaglini F, Viaggi C, Piro V, et al. Acetaldehyde and parkinsonism: role of CYP450 2E1. *Front Behav Neurosci*. 2013;7:71. doi:10.3389/fnbeh.2013.00071
13. Bromek E, Daniel WA. The regulation of liver cytochrome P450 expression and activity by the brain serotonergic system in different experimental models. *Expert Opin Drug Metab Toxicol*. 2021;17(4):413–424. doi:10.1080/17425255.2021.1872543
14. Ookhtens M, Kaplowitz N. Role of the liver in interorgan homeostasis of glutathione and cyst(e)ine. *Semin Liver Dis*. 1998;18(4):313–329. doi:10.1055/s-2007-1007167.
15. Lu SC. Regulation of glutathione synthesis. *Mol Aspects Med*. 2009;30(1–2):42–59. doi:10.1016/j.mam.2008.05.005.
16. Perry TL, Norman MG, Yong VW, et al. Hallervorden-Spatz disease: cysteine accumulation and cysteine dioxygenase deficiency in the globus pallidus. *Ann Neurol*. 1985;18(4):482–489. doi:10.1002/ana.410180411.
17. Squitti R, Gorgone G, Panetta V, et al. Implications of metal exposure and liver function in Parkinsonian patients resident in the vicinities of ferroalloy plants. *J Neural Transm*. 2009;116(10):1281–1287. doi:10.1007/s00702-009-0283-0
18. Shin HW, Park HK. Recent updates on acquired hepatocerebral degeneration. *Tremor Other Hyperkinet Mov*. 2017;7:463. doi:10.7916/D8TB1K44
19. Rose CF, Verkhratsky A, Parpura V. Astrocyte glutamine synthetase: pivotal in health and disease. *Biochem Soc Trans*. 2013;41(6):1518–1524. doi:10.1042/BST20130237
20. Sanderson E, Glymour MM, Holmes MV, et al. Mendelian randomization. *Nat Rev Meth Primers*. 2022;2:6. doi:10.1038/s43586-021-00092-5
21. Cheng Q, Zhang X, Chen LS, Liu J. Mendelian randomization accounting for complex correlated horizontal pleiotropy while elucidating shared genetic etiology. *Nat Commun*. 2022;13(1):6490. doi:10.1038/s41467-022-34164-1
22. Shin SY, Fauman EB, Petersen AK, et al. An atlas of genetic influences on human blood metabolites. *Nat Genet*. 2014:46,543–550. doi:10.1038/ng.2982
23. Sanderson E, Windmeijer F. A weak instrument [Formula: see text]-test in linear IV models with multiple endogenous variables. *J Econom*. 2016;190(2):212–221. doi:10.1016/j.jeconom.2015.06.004
24. Sanderson E, Spiller W, Bowden J. Testing and correcting for weak and pleiotropic instruments in two-sample multivariable Mendelian randomization. *Stat Med*. 2021;40(25):5434–5452. doi:10.1002/sim.9133
25. Burgess S, Butterworth A, Thompson SG. Mendelian randomization analysis with multiple genetic variants using summarized data. *Genet Epidemiol*. 2013;37(7):658–665. doi:10.1002/gepi.21758
26. Bowden J, Davey Smith G, Haycock PC, Burgess S. Consistent estimation in Mendelian randomization with some invalid instruments using a weighted median estimator. *Genet Epidemiol*. 2016;40(4):304–314. doi:10.1002/gepi.21965
27. Bowden J, Davey Smith G, Burgess S. Mendelian randomization with invalid instruments: effect estimation and bias detection through Egger regression. *Int J Epidemiol*. 2015;44(2):512–525. doi:10.1093/ije/dyv080
28. Yu G, Wang LG, Han Y, He QY. clusterProfiler: an R package for comparing biological themes among gene clusters. *OMICS*. 2012;16(5):284–287. doi:10.1089/omi.2011.0118
29. Hänzelmann S, Castelo R, Guinney J. GSVA: gene set variation analysis for microarray and RNA-seq data. *BMC Bioinf* 2013;14:7. doi:10.1186/1471-2105-14-7
30. Bindea G, Mlecnik B, Tosolini M, et al. Spatiotemporal dynamics of intratumoral immune cells reveal the immune landscape in human cancer. *Immunity*. 2013;39(4):782–795. doi:10.1016/j.immuni.2013.10.003
31. Zhao X, Zhang L, Wang J, et al. Identification of key biomarkers and immune infiltration in systemic lupus erythematosus by integrated bioinformatics analysis. *J Transl Med*. 2021;19(1):35. doi:10.1186/s12967-020-02698-x
32. Morris GM, Huey R, Olson AJ. Using AutoDock for ligand-receptor docking. *Curr Protoc Bioinformatics*. 2008;24. doi:10.1002/0471250953.bi0814s24
33. Wang Y, Bryant SH, Cheng T, et al. PubChem BioAssay: 2017 update. *Nucleic Acids Res*. 2017;45(D1):D955–D963. doi:10.1093/nar/gkw1118
34. Schwarting RK, Sedelis M, Hofele K, Auburger GW, Huston JP. Strain-dependent recovery of open-field behavior and striatal dopamine deficiency in the mouse MPTP model of Parkinson's disease. *Neurotox Res*. 1999;1(1):41–56. doi:10.1007/BF03033338
35. Huang ZP, Liu SF, Zhuang JL, et al. Role of microglial metabolic reprogramming in Parkinson's disease. *Biochem Pharmacol*. 2023;213:115619. doi:10.1016/j.bcp.2023.115619
36. Samidurai M, Palanisamy BN, Bargues-Carot A, et al. PKC delta activation promotes endoplasmic reticulum stress (ERS) and NLR family pyrin domain-containing 3 (NLRP3) inflammasome activation subsequent to asynuclein-induced microglial activation: involvement of thioredoxin-interacting protein (TXNIP)/Thioredoxin (Trx) redoxisome pathway. *Front Aging Neurosci*. 2021;13:661505. doi:10.3389/fnagi.2021.661505
37. Smith RL, Soeters MR, Wüst RCI, Houtkooper RH. Metabolic flexibility as an adaptation to energy resources and requirements in health and disease. *Endocr Rev*. 2018;39(4):489–517. doi:10.1210/er.2017-00211
38. Cunnane SC, Trushina E, Morland C, et al. Brain energy rescue: an emerging therapeutic concept for neurodegenerative disorders of ageing. *Nat Rev Drug Discov*. 2020;19(9):609–633. doi:10.1038/s41573-020-0072-x
39. Heiser C, Haller B, Sohn M, et al. Olfactory function is affected in patients with cirrhosis depending on the severity of hepatic encephalopathy. *Ann Hepatol*. 2018;17(5):822–829. doi:10.5604/01.3001.0012.3143
40. Mizuno K, Ueno Y. Autonomic nervous system and the liver. *Hepatol Res*. 2017;47(2):160–165. doi:10.1111/hepr.12760
41. Denson LA, Jurickova I, Karns R, et al. Clinical and genomic correlates of neutrophil reactive oxygen species production in pediatric patients with Crohn's disease. *Gastroenterology*. 2018;154(8):2097–2110. doi:10.1053/j.gastro.2018.02.016
42. Gámez-Belmonte R, Hernández-Chirlaque C, Sánchez de Medina F, Martínez-Augustin O. Experimental acute pancreatitis is enhanced in mice with tissue nonspecific alkaline phosphatase haplodeficiency due to modulation of neutrophils and acinar cells. *Biochim Biophys Acta Mol Basis Dis*. 2018;1864(11):3769–3779. doi:10.1016/j.bbadis.2018.09.009
43. Li J, Du Q, Sun J, Xiang L, Wang S. Identification and validation of a novel phagocytosis regulators-related signature with potential prognostic and immunotherapeutic value in patients with lung adenocarcinoma. *Front Oncol*. 2022;12:988332. doi:10.3389/fonc.2022.988332
44. Wang L, Aschenbrenner D, Zeng Z, et al. Gain-of-function variants in SYK cause immune dysregulation and systemic inflammation in humans and mice. *Nat Genet*. 2021;53(4):500–510. doi:10.1038/s41588-021-00803-4
45. Cao QQ, Li S, Lu Y, et al. Transcriptome analysis of molecular mechanisms underlying facial nerve injury repair in rats. *Neural Regen Res*. 2021;16(11):2316–2323. doi:10.4103/1673-5374.310700
46. Pajares M, Rojo I, Manda A, G BL, Cuadrado A. Inflammation in Parkinson's disease: mechanisms and therapeutic implications. *Cells*. 2020;9(7):1687. doi:10.3390/cells9071687

47. Ferrari CC, Tarelli R. Parkinson's disease and systemic inflammation. *Parkinson's Dis*. 2011;2011:436813. doi:10.4061/2011/436813
48. Gopinath A, Mackie PM, Phan LT, Tansey MG, Khoshbouei H. The complex role of inflammation and gliotransmitters in Parkinson's disease. *Neurobiol Dis*. 2023;176:105940. doi:10.1016/j.nbd.2022.105940
49. Borges N. Tolcapone-related liver dysfunction: implications for use in Parkinson's disease therapy. *Drug Saf*. 2003;26(11):743–747. doi:10.2165/00002018-200326110-00001
50. Wang X, Liang T, Mao Y, et al. Nervonic acid improves liver inflammation in a mouse model of Parkinson's disease by inhibiting proinflammatory signaling pathways and regulating metabolic pathways. *Phytomedicine*. 2023;117:154911. doi:10.1016/j.phymed.2023.154911
51. Lv J, Xiao Q, Chen Y, et al. Effects of magnesium isoglycyrrhizinate on AST, ALT, and serum levels of Th1 cytokines in patients with allo-HSCT. *Int Immunopharmacol*. 2017;46:56–61. doi:10.1016/j.intimp.2017.02.022
52. Niculescu DA, Dusceac R, Galoiu SA, Capatina CA, Poiana C. SERIAL CHANGES OF LIVER FUNCTION TESTS BEFORE AND DURING METHIMAZOLE TREATMENT IN THYROTOXIC PATIENTS. *Endocr Pract*. 2016;22(8):974–979. doi:10.4158/EP161222.OR
53. Prasad EM, Hung SY. Behavioral tests in neurotoxin-induced animal models of Parkinson's disease. *Antioxidants*. 2020;9(10):1007. doi:10.3390/antiox9101007
54. Thakar JH, Hassan MN. Effects of 1-methyl-4-phenyl-1,2,3,6-tetrahydropyridine (MPTP), cyperquat (MPP+) and paraquat on isolated mitochondria from rat striatum, cortex and liver. *Life Sci*. 1988;43(2):143–149. doi:10.1016/0024-3205(88)90291-3
55. Datta I, Mekha SR, Kaushal A, Ganapathy K, Razdan R. Influence of intranasal exposure of MPTP in multiple doses on liver functions and transition from non-motor to motor symptoms in a rat PD model. *Naunyn Schmiedebergs Arch Pharmacol*. 2020;393(2):147–165. doi:10.1007/s00210-019-01715-1

Journal of Inflammation Research

Dovepress
Taylor & Francis Group

Publish your work in this journal

The Journal of Inflammation Research is an international, peer-reviewed open-access journal that welcomes laboratory and clinical findings on the molecular basis, cell biology and pharmacology of inflammation including original research, reviews, symposium reports, hypothesis formation and commentaries on: acute/chronic inflammation; mediators of inflammation; cellular processes; molecular mechanisms; pharmacology and novel anti-inflammatory drugs; clinical conditions involving inflammation. The manuscript management system is completely online and includes a very quick and fair peer-review system. Visit http://www.dovepress.com/testimonials.php to read real quotes from published authors.

Submit your manuscript here: https://www.dovepress.com/journal-of-inflammation-research-journal